utilizes autophagic membrane as a site of genome replication, whereas influenza virus attenuates apoptosis through the induction of autophagy (10, 59). Moreover, several groups have reported that HCV induces autophagy for infection or replication (5, 49); however, the role(s) of autophagy in the propagation of HCV is still controversial and the involvement of autophagy in the pathogenesis of HCV has not yet been clarified. In this study, we examined the biological significance of the autophagy observed in cells in which the HCV genome replicates.

MATERIALS AND METHODS

Plasmids. The plasmids pmStrawberry-C1, pmStrawberry-Atg4B^{C74A}, pmRFP-GFP-LC3, pEGFP-LC3, and pEGFP-Atg16L were described previously (7, 8, 24). The plasmids pFGR-JFH1 and pSGR-JFH1 were kind gifts from T. Wakita.

Cell culture. All cell lines were cultured at 37°C under a humidified atmosphere with 5% CO_2. Huh7 cells were cultivated in Dulbecco's modified Eagle's medium (DMEM) supplemented with 10% fetal bovine serum (FBS), nonessential amino acids, 100 U/ml penicillin, and 100 mg/ml streptomycin. For the starvation, the cells were cultivated with Earle's balanced salt solution (EBSS) (Sigma) for 6 h. HCV replicon cells were established as described previously (53). The plasmid pairs pFK-I$_{389}$ neo/NS3-3′/NK5.1 and pFK-I$_{389}$ neo/FGR/NK5.1 and pFGR-JFH1 and pSGR-JFH1 were linearized with ScaI or XbaI. The plasmids pFGR-JFH1 and pSGR-JFH1 were treated with mung bean exonuclease. The linearized DNA was transcribed *in vitro* by using the MEGAscript T7 kit (Applied Biosystems) according to the manufacturer's protocol. The transcribed RNA was electroporated into cells under conditions of 270 V and 960 mF using a Gene Pulser (Bio-Rad). All HCV replicon cells were maintained in DMEM containing 10% FBS, nonessential amino acids, and 1 mg/ml G418 (Nacalai).

Reagents and antibodies. Concanamycin A and bafilomycin A1 were purchased from Sigma and Fluka, respectively. E64D and pepstatin A were from Peptide Institute Inc. Rabbit anti-HCV NS5A polyclonal antibody was described previously (45). Mouse monoclonal anti-JEV NS3 antibody was prepared by immunization using the recombinant protein spanning amino acid residues 171 to 619 of JEV NS3. Rabbit polyclonal anti-LC3 (PM036), mouse monoclonal anti-RFP (8D6), and anti-62/SQSTM1 (5F2) antibodies were purchased from Medical & Biological Laboratories. Rabbit polyclonal anti-cathepsin B (FL-339) and mouse monoclonal anti-LAMP1 (H4A3) antibodies were from Santa Cruz Biotechnology. Mouse monoclonal anti-HCV NS5A (HCM-131-5), rabbit polyclonal anti-β-actin, and mouse monoclonal anti-Golgin97 (CDF4) antibodies were from Austral Biologicals, Sigma, and Invitrogen, respectively. Mouse monoclonal and rabbit polyclonal anti-cathepsin B antibodies were from Calbiochem. Mouse monoclonal anti-p62/SQSTM1 (5F2) and anti-ATP6V0D1 (ab56441) antibodies were from Abcam. Rabbit polyclonal anti-Atg4B antibody was from Sigma. Mouse anti-double-stranded RNA (dsRNA) IgG2a (J2 and K1) antibodies were from Biocenter Ltd. (Szirak, Hungary).

Transfection, infection, and immunoblotting. Transfection and infection were carried out as described previously (53). Each lysosome-enriched fraction was isolated by using the Lysosome Enrichment Kit for Tissue and Cultured Cells (Pierce) according to the manufacturer's protocol. Samples were subjected to 12.5% sodium dodecyl sulfate-polyacrylamide gel electrophoresis. The proteins were transferred to polyvinylidene difluoride membranes (Millipore) and were reacted with the appropriate antibodies. The immune complexes were visualized with Super Signal West Femto substrate (Pierce) and detected by an LAS-3000 image analyzer system (Fujifilm). The protein bands of LC3 and β-actin were quantified by Multi Gauge software (Fujifilm), and the values of LC3 were normalized to those of β-actin.

Fluorescence microscopy. Cells were cultured on glass slides and then fixed with 4% paraformaldehyde in phosphate-buffered saline (PBS) at room temperature for 30 min. After being washed twice with PBS, the cells were permeabilized at room temperature for 20 min with PBS containing 0.25% saponin and then blocked with PBS containing 0.2% gelatin (gelatin-PBS) for 60 min at room temperature. The cells were incubated with gelatin-PBS containing appropriate antibodies at 37°C for 60 min and washed three times with PBS containing 1% Tween 20 (PBST). The resulting cells were incubated with gelatin-PBS containing corresponding fluorescent-conjugated secondary antibodies at 37°C for 60 min and then washed three times with PBST. The stained cells were covered with Vectashield mounting medium containing DAPI (4′,6-diamidino-2-phenylindole) (Vector Laboratories Inc.) and observed with a FluoView FV1000 laser scanning confocal microscope (Olympus). Time-lapse video microscopy was performed at 37°C with a DeltaVision microscope system (Applied Precision Inc.) equipped with a ΔTC3 culture dish system (Bioptechs) for temperature control.

Quantification of pro-cathepsin B. Each cell line was seeded on 12-well type I collagen-coated dishes (IWAKI) and cultured for 48 h. The supernatant and the cells were harvested and subjected to quantification of pro-cathepsin B by using Quantikine human pro-cathepsin B immunoassay (R&D Systems) according to the manufacturer's protocol.

Statistical analysis. Estimated values were represented as the means ± standard deviations. The significance of differences in the means was determined by Student's *t* test.

RESULTS

Autophagy is induced in the HCV replicating cell in a strain-dependent manner. To determine whether autophagy is induced during the replication of HCV, we investigated the phosphoethanolamine (PE) conjugation of LC3 in HCV replicon cells in which HCV RNA was autonomously replicating. As shown in Fig. 1A, the amounts of PE-conjugated LC-3 (LC3-II), a conventional marker for an autophagosomal membrane, in Huh7 cells were slightly increased by starvation, in conjunction with a reduction of the unmodified LC-3 (LC3-I). In contrast, the amount of LC3-II was significantly increased in the subgenomic and full genomic HCV replicon cells of the genotype 1b strain Con1 (SGR^{Con1} and FGR^{Con1}), whereas a small amount of LC3-II was detected in the full genomic replicon cells of the genotype 2a strain JFH1 (FGR^{JFH1}). We also examined the subcellular localization of LC3 by using confocal microscopy. Although LC3 was diffusely detected in the cytoplasm of naïve Huh7 cells, small foci of the accumulated LC3 appeared after starvation (Fig. 1B), whereas many LC3 foci that were larger in size than those in the starved cells appeared in the cytoplasm, particularly near the nucleus, in both SGR^{Con1} and FGR^{Con1} cells. However, a low level of LC3 focus formation comparable to that in the starved cells was observed in the FGR^{JFH1} cells. Most of the LC3 foci were not colocalized with NS5A, an HCV protein of the viral replication complex, in the HCV replicon cells, as reported previously (49). Elimination of HCV RNA from the SGR^{Con1} cells by treatment with alpha interferon (SGR^{cured}) abrogated the lipidation and accumulation of LC3 (Fig. 1C and D). Interestingly, overexpression of the HCV polyprotein of genotype 1b by an expression plasmid induced no autophagy (data not shown), suggesting that replication of viral RNA is required for induction of autophagy. Furthermore, neither lipidation nor accumulation of LC3 was observed in SGR^{JEV} cells harboring subgenomic replicon RNA cells of Japanese encephalitis virus (JEV), which is also a member of the family *Flaviviridae* (Fig. 1C and D). These results suggest that replication of HCV but not that of JEV induces autophagy.

The autophagy flux is impaired in the replicon cells of HCV strain Con1 after a step of autophagosome formation. To further examine the autophagy induced in the HCV replicon cells in more detail, Huh7 and SGR^{Con1} cells were treated with pepstatin A and E64D, inhibitors of aspartic protease and cysteine protease, respectively. In this assay, treatment of intact cells capable of inducing autophagy with the inhibitors increases the amount of LC3-II, whereas no increase is observed in cells impaired in the autophagic degradation. The amount of LC3-II was significantly increased in the naïve Huh7

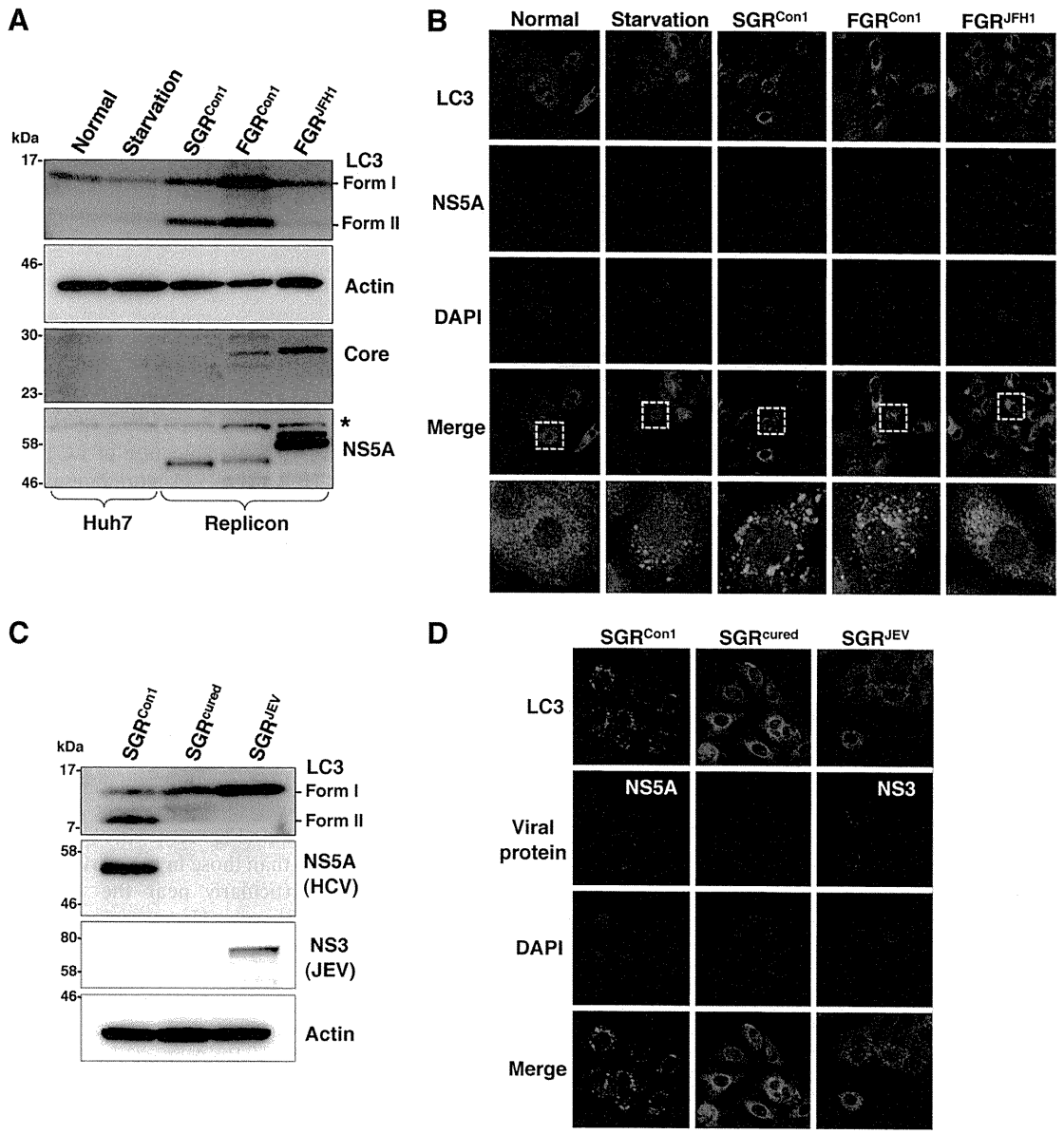

FIG. 1. Induction of autophagy in the HCV replicon cells. (A) The starved Huh7 cells and HCV replicon cells harboring a sub- or full genomic RNA of strain Con1 or strain JFH1 were subjected to immunoblotting using the appropriate antibodies. The asterisk indicates a nonspecific band. (B) Subcellular localizations of LC3 and NS5A were determined by confocal microscopy. The replicon cells and the starved Huh7 cells were stained with DAPI and then reacted with rabbit polyclonal anti-LC3 and mouse monoclonal anti-NS5A antibodies, respectively, followed by Alexa Fluor 488- and 594-conjugated secondary antibodies, respectively. The boxed areas in the merged images are magnified. (C) SGR^{Con1} cells were treated with alpha interferon for 1 week to remove the HCV replicon RNA. The resulting cells were designated SGR^{cured} cells. The SGR^{Con1}, SGR^{cured}, and SGR^{JEV} cells were lysed and subjected to immunoblotting using the appropriate antibodies. (D) Subcellular localization of LC3 and JEV NS3 and HCV NS5A was determined by confocal microscopy after staining with DAPI, followed by staining with rabbit polyclonal anti-LC3 and anti-JEV NS3 antibodies and mouse monoclonal anti-NS5A antibodies and then with the appropriate secondary antibodies. The data shown are representative of three independent experiments.

cells by treatment with the inhibitors, whereas only a slight increase was observed in the SGR^{Con1} cells (5.4-fold versus 1.6-fold) (Fig. 2A), suggesting that autophagy is suppressed in the HCV replicon cells. Furthermore, cytoplasmic accumulation of LC3 was significantly increased in the naïve Huh7 cells by treatment with the inhibitors, in contrast to the only slight increase induced by treatment in the SGR^{Con1} cells (Fig. 2B). In SGR^{Con1} cells, the LC3 foci were colocalized with the polyubiquitin-binding protein p62/SQSTM1, a specific substrate for autophagy (18), suggesting that most of the autophagosomes were distributed in the cytoplasm of the SGR^{Con1} cells (Fig. 2B and C). Next, to examine the autophagy flux in the SGR^{Con1} cells, we monitored the green fluorescent protein (GFP)-conjugated LC3 dynamics in living cells by using time-lapse imaging techniques (see movies in the supplemental material). A large number of small GFP-LC3 foci were detected in the

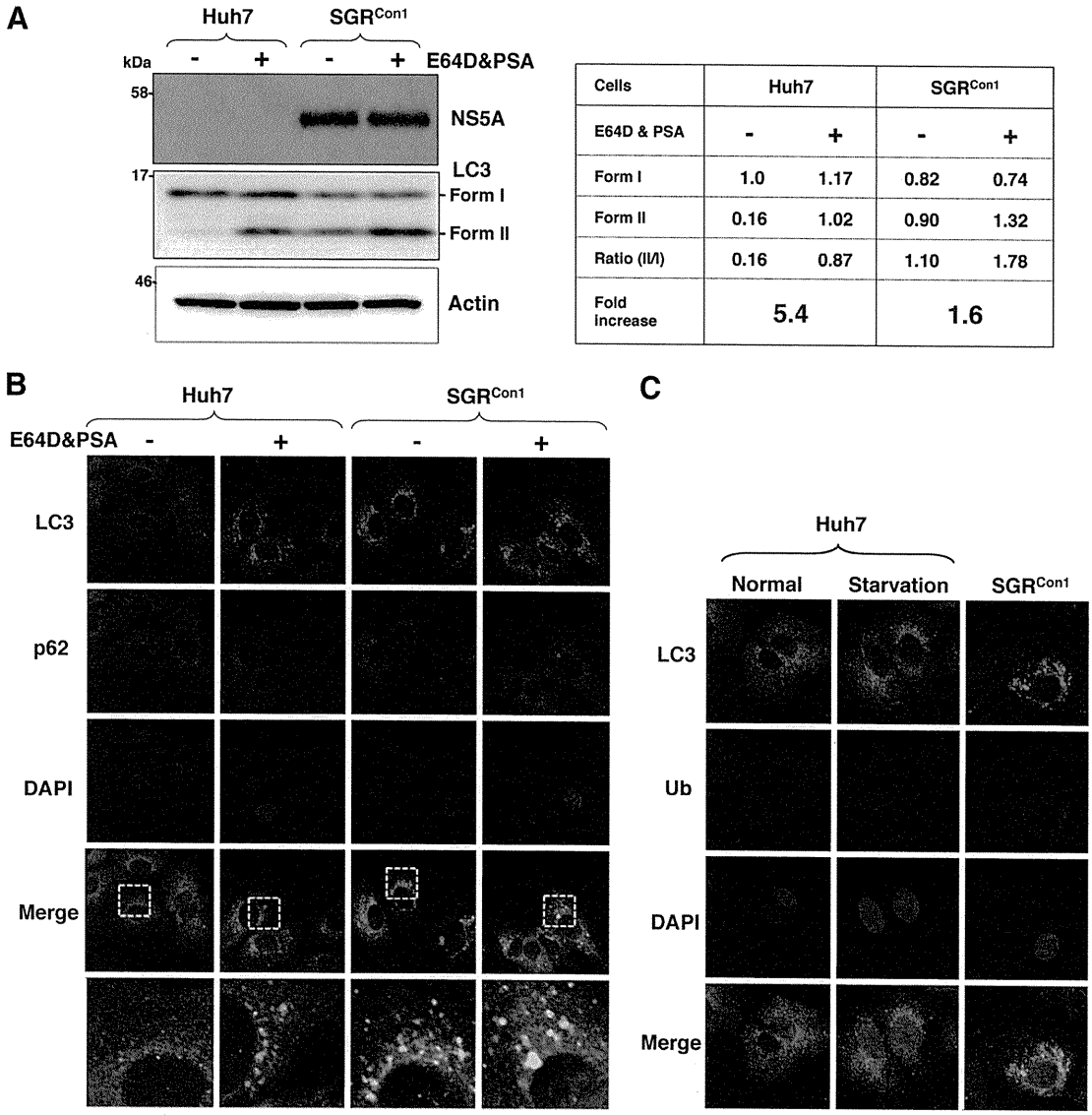

Cells	Huh7		SGR^{Con1}	
E64D & PSA	-	+	-	+
Form I	1.0	1.17	0.82	0.74
Form II	0.16	1.02	0.90	1.32
Ratio (II/I)	0.16	0.87	1.10	1.78
Fold increase	5.4		1.6	

FIG. 2. Autophagy flux is impaired in the HCV replicon cells. Autophagy flux assay using lysosomal protease inhibitors. (A) Huh7 and SGR^{Con1} cells were treated with 20 μM E64D and pepstatin A (PSA) for 6 h, and the cell lysates were subjected to immunoblotting. The density of the protein band was estimated by Multi Gauge version 2.2 (Fujifilm). (B) After nuclear staining with DAPI, the intracellular localizations of LC3 and p62 in each cell were determined by staining with rabbit polyclonal anti-LC3 and mouse monoclonal anti-62 antibodies, respectively, followed by staining with Alexa Fluor 488- and 594-conjugated secondary antibodies, respectively. The resulting cells were observed by confocal microscopy. (C) Colocalization of accumulated LC3 with ubiquitinated proteins (Ub) in SGR^{Con1} cells. Nontreated and starved Huh7 cells and SGR^{Con1} cells were fixed and stained with DAPI and rabbit anti-LC3 and anti-ubiquitin (6C1.17) (BD) polyclonal antibodies, respectively, and then with the appropriate secondary antibodies. Subcellular localizations of LC3 and Ub were determined by confocal microscopy. The data shown are representative of three independent experiments.

starved Huh7 cell, moved quickly, and finally disappeared within 30 min. Although small foci of GFP-LC3 exhibited characteristics similar to those in the starved cells, some large foci exhibited confined movement and maintained constant fluorescence for at least 3 h in the SGR^{Con1} cells. The GFP-LC3 foci in the SGR^{JFH1} cells showed characteristics similar to those in the starved cells. These results support the notion that autophagy flux is suppressed in the SGR^{Con1} cells at some step after autophagosome formation.

Impairment of autolysosomal acidification causes incomplete autophagy in the replicon cell of strain Con1. Recent studies have shown that some viruses inhibit the autophagy pathway by blocking the autolysosome formation (10, 42). Therefore, we determined the autolysosome formation in the HCV replicon cells through the fusion of autophagosome with lysosome. Colocalization of small foci of LC3 with LAMP1, a lysosome marker, was observed in the starved Huh7 cells, SGR^{Con1} cells, and SGR^{JFH1} cells but not in the SGR^{cured} cells (Fig. 3A), suggesting that autolysosomes are formed in the HCV replicon cells of both Con1 and JFH1 strains. The autolysosome is acidified by the vacuolar-type H^+ ATPase (V-ATPase) and degrades substrates by the lysosomal acidic hy-

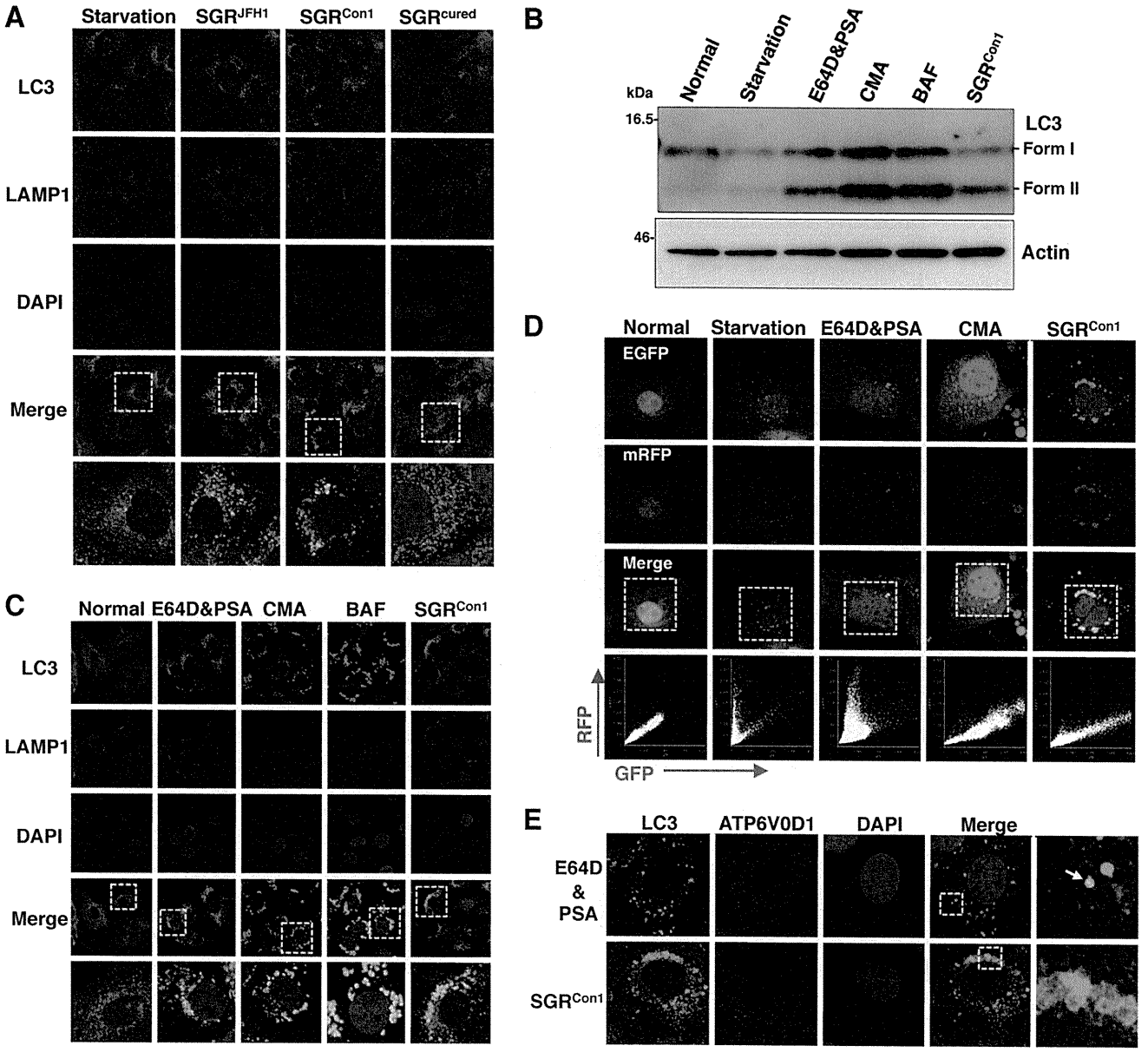

FIG. 3. Inhibition of autophagy maturation in HCV replicon cells. (A) After nuclear staining with DAPI, starved Huh7 cells, replicon cells, and SGR^{cured} cells were stained with rabbit polyclonal anti-LC3 and mouse monoclonal anti-LAMP1 antibodies followed by Alexa Fluor 488- and 594-conjugated secondary antibodies, respectively, and examined by confocal microscopy. The boxed regions in the merged images are magnified. (B and C) Huh7 cells were treated with 20 μM protease inhibitors (E64D and PSA) or a 20 nM concentration of a V-ATPase inhibitor (CMA or BAF) for 6 h. (B) Cell lysates were subjected to immunoblotting using antibodies against LC3 and β-actin. (C) Intracellular localization of LAMP1 and LC3 was determined by confocal microscopy after staining with DAPI and appropriate antibodies. The boxed areas in the merged images are magnified. (D) Tandem fluorescence-tagged LC3 assay. The expression plasmid encoding mRFP-GFP-tandem-tagged LC3 was transfected into naïve and starved Huh7 cells or into the SGR^{Con1} cells treated with the indicated inhibitors at 36 h posttransfection. The resulting cells were fixed at 42 h posttransfection, and the relative GFP and RFP signals were determined by confocal microscopy. The fluorescent values in the boxes of the merged images were determined and shown as dot plots in the bottom column of the grid, in which the *x* and *y* axes indicate the signals of GFP and RFP, respectively. (E) Huh7 cells treated with E64D and PSA and the SGR^{Con1} cells were stained with DAPI and then with rabbit polyclonal anti-LC3 and mouse monoclonal anti-ATP6V0D1 antibodies followed by Alexa Fluor 488- and 594-conjugated secondary antibodies, respectively. The boxed regions in the merged images are magnified. A white arrow indicates colocalization of LC3 and ATP6V0D1. The data shown are representative of three independent experiments.

drolases in the vesicle (2). Next, to determine the possibility of a deficiency in the acidification of the autolysosome on the autophagic dysfunction in the Con1 replicon cells, Huh7 cells were treated with the protease inhibitors E64D and pepstatin A (PSA) or with each of the V-ATPase inhibitors concanamycin A (CMA) and bafilomycin A1 (BAF). The amount of LC3-II was significantly increased in Huh7 cells treated with the inhibitors just as in the SGR^{Con1} cells (Fig. 3B). Further-

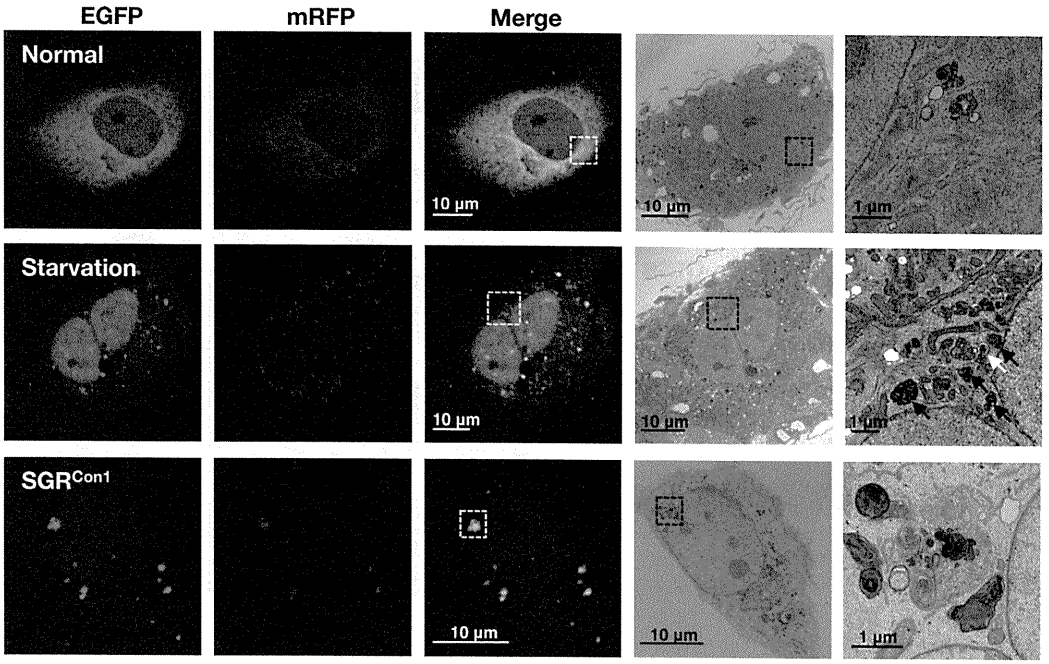

FIG. 4. Correlative fluorescence microscopy-electron microscopy (FM-EM) analysis. The expression plasmid encoding mRFP-GFP-tandem-tagged LC3 was transfected into naïve and starved Huh7 cells or into the SGR^{Con1} cells as described in the legend to Fig. 3D, and the mRFP-GFP-tandem-tagged LC3 signals were observed at 36 h posttransfection. The boxed regions in the merged images are magnified. The data shown are representative of three independent experiments.

more, the large foci of LC3 colocalized with LAMP1 appeared in the cells treated with the V-ATPase inhibitors, as seen in SGR^{Con1} cells (Fig. 3C). These results suggest that stacked autophagosome flux caused by the inhibition of lysosomal degradation or acidification exhibits characteristics similar to those observed in the Con1 replicon cells.

Since the fluorescence of GFP but not that of monomeric red fluorescent protein (mRFP) disappears under the acidic environment, expression of mRFP-GFP tandem fluorescent-tagged LC3 (tfLC3) is capable of being used to monitor the acidic status of the autolysosome (24). Both GFP and mRFP fluorescent signals were unfused, some of them accumulated as small foci in Huh7 cells after starvation or by treatment with the protease inhibitors, and half of the foci of mRFP were not colocalized with those of GFP (Fig. 3D), indicating that half of the foci are in an acidic state due to maturation into an autolysosome after fusion with a lysosome. On the other hand, the large foci of GFP and mRFP were completely colocalized in Huh7 cells treated with CMA or in the SGR^{Con1} cells. These results suggest that the large foci of LC3 in the SGR^{Con1} cells are not under acidic conditions. Recently, it was shown that the lack of lysosomal acidification in human genetic disorders due to dysfunction in assembly/sorting of V-ATPase induces incomplete autophagy similar to that observed in SGR^{Con1} cells (31, 45). Therefore, to explore the reason for the lack of acidification of the autolysosome in the SGR^{Con1} cells, we examined the subcellular localization of ATP6V0D1, a subunit of the integral membrane V_0 complex of V-ATPase. Colocalization of ATP6V0D1 with large foci of LC3 was observed in Huh7 cells treated with the protease inhibitors but not in SGR^{Con1} cells (Fig. 3E), suggesting that dislocation of V-ATPase may participate in the impairment of the autolysosomal acidification in the SGR^{Con1} cells.

We further examined the morphological characteristics of the LC3-positive compartments by using correlative fluorescence microscopy-electron microscopy (FM-EM) (Fig. 4). The starved Huh7 cells exhibited a small double-membrane vesicle (white arrow) and high-density single-membrane structures (black arrows) in close proximity to the correlative position of the GFP- and mRFP-positive LC3 compartments, which are considered to be the autophagosome and lysosome/autolysosome, respectively. In contrast, many high-density membranous structures were detected in the correlative position of the large GFP- and mRFP-positive LC3 compartment in the SGR^{Con1} cells, which is well consistent with the observation in the time-lapse imaging in which small foci of LC3 headed toward and assembled with the large LC3-positive compartment (see movies in the supplemental material). These results suggest that the formation of large aggregates with aberrant inner structures in the SGR^{Con1} cells may impair maturation of the autolysosome through the interference of further fusion with functional lysosomes for the degradation.

The secretion of immature cathepsin B is enhanced in the replicon cell of strain Con1. Lysosomal acidification is required for the cleavage of cathepsins for activation, and cathepsin B (CTSB) is processed under acidic conditions (13). Although a marginal decrease of CTSB was detected in the whole lysates of the SGR^{Con1} cells, a significant reduction in the expression of both unprocessed (pro-CTSB) and matured CTSB was observed in the lysosomal fractions of the SGR^{Con1} cells compared with those of the naïve Huh7 and the SGR^{cured} cells (Fig. 5A). LAMP1 was concentrated at a similar level in

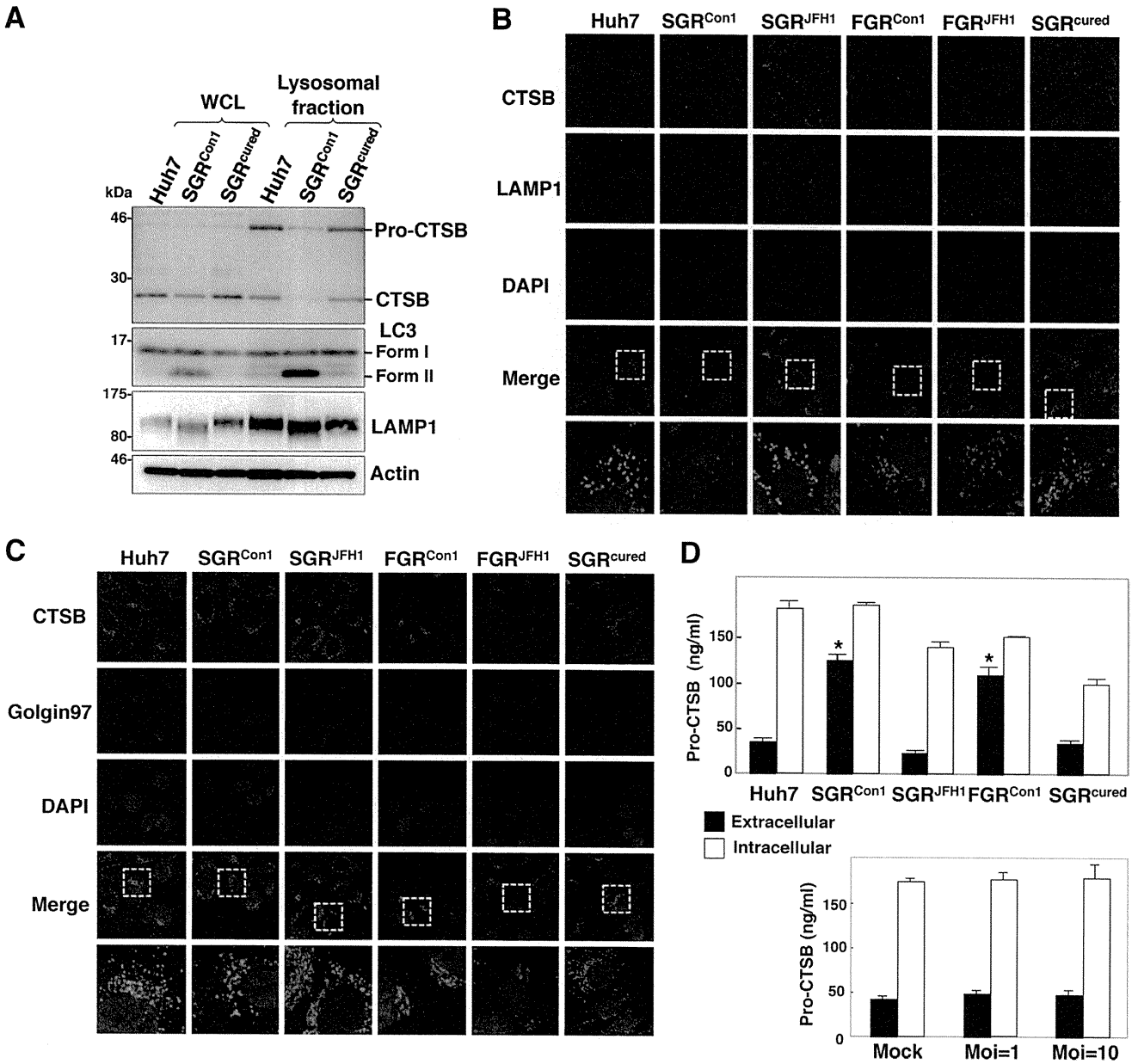

FIG. 5. Enhanced secretion of pro-CTSB in the HCV replicon cells. (A) The whole-cell lysate (WCL) and lysosomal fraction prepared from Huh7, SGR^{Con1}, and SGR^{cured} cells were subjected to immunoblotting. (B and C) Huh7 cells, HCV replicon cells, and SGR^{cured} cells were stained with DAPI, rabbit polyclonal anti-CTSB antibody, and mouse anti-LAMP1 (B) or anti-Golgin97 (C) antibody. The boxed areas in the merged images are magnified. (D) Expression of pro-cathepsin B in the culture supernatants (black bars) and cell lysates (white bars) of the Huh7, SGR^{Con1}, SGR^{JFH1}, FGR^{Con1}, and SGR^{cured} cells and the SGR^{cured} cells infected with HCVcc at a multiplicity of infection (Moi) of 1 or 10 and incubated for 72 h was determined by enzyme-linked immunosorbent assay (ELISA). The error bars indicate standard deviations. The asterisks indicate significant differences ($P < 0.01$) versus the control value. The data shown are representative of three independent experiments.

the lysosomal fractions of the cells, whereas LC-II was detected in the fractions of the SGR^{Con1} cells but not in those of Huh7 and the SGR^{cured} cells, suggesting that autophagosomes and/or autolysosomes in the SGR^{Con1} cells are fractionated in the lysosomal fraction. Colocalization of CTSB with LAMP1 was observed in the naïve Huh7 cells, in the SGR^{cured} cells, and in the replicon cells harboring a sub- or a full genomic RNA of strain JFH1 (SGR^{JFH1} and FGR^{JFH1}, respectively) but not in those of strain Con1 (SGR^{Con1} and FGR^{Con1}) (Fig. 5B). On the other hand, CTSB was colocalized with Golgin97, a marker for the Golgi apparatus, in the SGR^{Con1} and FGR^{Con1} cells but not in other cells (Fig. 5C). Since previous reports suggested that the alkalization in the lysosome triggers secretion of the unprocessed lysosomal enzymes (19, 41), we next determined the secretion of pro-CTSB in the replicon cells. Secretion of the pro-CTSB was significantly enhanced in the replicon cells of strain Con1 but not in those of strain JFH1 and naïve and cured cells (Fig. 5D, top). Furthermore, secretion of pro-CTSB

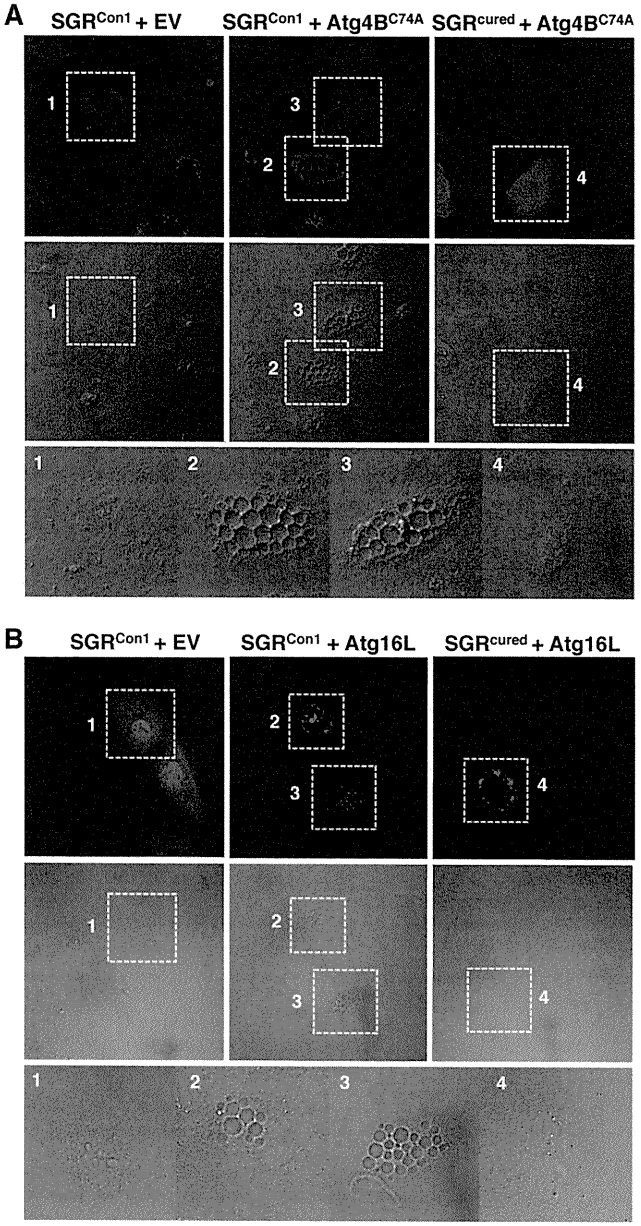

FIG. 6. Inhibition of autophagosome formation induces severe cytoplasmic vacuolations leading to cell death in the HCV replicon cells. (A) SGR^{Con1} and SGR^{cured} cells transfected with pStrawberry-$Atg4B^{C74A}$ or empty vector pStrawberry (EV) were fixed at 48 h posttransfection and examined by fluorescence microscopy. The boxed areas in the phase-contrast images are magnified. (B) SGR^{Con1} and SGR^{cured} cells transfected with pEGFP-Atg16L or EV were examined by fluorescence microscopy at 48 h posttransfection. The boxed areas in the phase-contrast images are magnified. (C) SGR^{cured}, SGR^{Con1}, and SGR^{cured} cells infected with JFH1 virus were transfected with pStrawberry-$Atg4B^{C74A}$, and the number of vacuole-positive cells in each of nine fields of view was counted at 48 h posttransfection. (D) SGR^{cured}, SGR^{Con1}, and SGR^{cured} cells infected with JFH1 virus were transfected with pStrawberry-$Atg4B^{C74A}$ (black bars) or EV (white bars), and cell viability was determined at 6 days posttransfection by using CellTiter-Glo (Promega) according to the manufacturer's protocol. The asterisks indicate significant differences ($P < 0.05$) versus the control value. The data shown are representative of three independent experiments.

was not observed in the cured cells infected with HCVcc, an infectious HCV strain derived from strain JFH1 (Fig. 5D, bottom). Collectively, these results suggest that the dysfunction of lysosomal acidification contributes to the impairment of autophagy in the HCV replicon cells of strain Con1.

Autophagy induced in cells replicating HCV is required for cell survival. Finally, we examined the pathological significance of autophagy during HCV replication. Atg4B is known as an LC3-processing protease, and overexpression of its protease-inactive mutant ($Atg4B^{C74A}$) results in inhibition of the autophagosome formation (7). To our surprise, severe cytoplasmic vacuolation was observed in the SGR^{Con1} cells expressing $Atg4B^{C74A}$ (Fig. 6A). These vacuolations were also observed in the SGR^{Con1} cells by the expression of Atg16L (Fig. 6B), a molecule that is an essential component of the autophagy complex and that, if expressed in excess amounts, can disrupt the autophagosome formation (8). Expression of $Atg4B^{C74A}$ induced a higher level of vacuole formation in the Con1 replicon cells than in cells infected with JFH1 virus but not in the cured cells (Fig. 6C). Along with these vacuolations, cell viability was significantly decreased by the expression of $Atg4B^{C74A}$ in SGR^{Con1} cells and slightly in JFH1 virus-infected cells (Fig. 6D). These results suggest that autophagy induced by the RNA replication of HCV is required for host cell survival.

DISCUSSION

In the present study, we demonstrated that two genotypes of HCV induce autophagy, whereas intact autophagy flux is required for the host cell to survive. The cell death characterized by cytoplasmic vacuolation that was induced in the HCV replicon cells by the inhibition of the autophagosome formation is similar to type III programmed cell death, which is distinguishable from apoptosis and autophagic cell death (4). Type III programmed cell death has been observed in the neurodegenerative diseases caused by the deposit of cytotoxic protein aggregates (15).

We previously reported that HCV hijacks chaperone complexes, which regulates quality control of proteins into the membranous web for circumventing unfolded protein response during efficient genome replication (53); in other words, the replication of HCV exacerbates the generation of proteins associated with cytotoxicity. In the experiments using a chimpanzee model, HCV of genotype 1 was successfully used to reproduce acute and chronic hepatitis similar to that in the human patients (3, 57), and transgenic mice expressing viral proteins of HCV of genotype 1b have been shown to develop

Sjögren syndrome, insulin resistance, hepatic steatosis, and hepatocellular carcinoma (27, 28). In contrast, HCVcc, based on the genotype 2a strain JFH1 isolated from a patient with fulminant hepatitis C (33, 56), was unable to establish chronic infection in chimpanzees (56) or to induce cell damage and inflammation in chimeric mice xenotransplanted with human hepatocytes (17). These results imply that the onset of HCV pathogenesis could be dependent not only upon an amount but also on a property of deposited proteins, and they might explain the aggravated vacuolations under the inhibition of autophagosome formation in strain Con1 compared to that in strain JFH1. Interestingly, the overexpression of $Atg4B^{C74A}$ or Atg16L causes eccentric cell death in the Con1 replicon cells in which autophagy flux is already disturbed. Thus, we speculated that the quarantine of undefined abnormalities endowed with high cytotoxicity by the engulfing of the autophagic membrane might be sufficient for the amelioration of HCV-induced degeneration. The autophagosomal dysfunction observed in the Con1 replicon cells may suggest that a replicant of strain Con1 was more sensitive to the lysosomal vacuolation than that of strain JFH1. Because a limitation of our study was that we were unable to use infectious HCV of other strains, it is still unclear whether the autophagic degradation can be impaired only in the replicon of HCV strain Con1 or genotype 1.

We also demonstrated that HCV replication of strain Con1 but not that of strain JFH1 facilitates the secretion of pro-CTSB. It has been well established that the secretion of pro-CTSB is enhanced in several types of tumors (26, 50). The secretion of CTSB, like the secretion of matrix metalloproteases, is a marker of the progression of the proteolytic degradation of the extracellular matrix, which plays an important part in cancer invasion and metastasis. Since infection with HCV of genotype 1 is clinically considered a risk factor for the development of hepatocellular carcinoma (14, 51), the enhanced secretion of pro-CTSB by the replication of genotype 1 strains might synergistically promote infiltration of hepatocellular carcinoma.

As shown elsewhere (see movies in the supplemental material), although most degradations of the autophagosome were impaired due to a dislocalization of a V-ATPase subunit, some autophagic degradation was achieved in the SGR^{Con1} cells similar to that in the starved Huh7 cells. Moreover, the stagnated autophagy flux was rescued by the treatment of alpha interferon accompanied by elimination of HCV (Fig. 1C and D). Interestingly, we observed neither a significant impairment of lysosomal degradation nor the intracellular activity of cathepsins in the replicon cells of HCV strain Con1 (data not shown). Therefore, there might be a specific dysfunction within the autolysosome during the replication of HCV strain Con1. Detailed studies are needed to elucidate how HCV strain Con1 disturbs the sorting of V-ATPase.

A close relationship between autophagy and the immune system has been gradually unveiled (47). Autophagy assists not only in the direct elimination of pathogens by hydrolytic degradation but also in antigen processing in antigen-presenting cells such as macrophage and dendritic cells (DC) for presentation by major histocompatibility complex (MHC) I and II (11). Moreover, autophagy plays important roles in T lymphocyte homeostasis (44). As such, in some instances, interruptions of autophagy can allow microorganisms to escape from the host immune system. Indeed, the immune response against herpes simplex virus was suppressed by blocking the autophagy (6). With regard to HCV, functionally impaired DC dysfunctions marked by poor DC maturation, impaired antigen presentation, and attenuated cytokine production have been reported in tissue culture models and chronic hepatitis C patients (1, 22, 46). In addition, reduction of cell surface expression of MHC-I in HCV genotype 1b replicon cells has been reported (55). We confirmed that levels of cell surface expression of MHC-I in the replicon cells of genotype 1b, but not of genotype 2a, were reduced in comparison with those in the cured cells (data not shown). Hence it might be feasible to speculate that the replication of HCV RNA of genotype 1 induces an incomplete autophagy for attenuating antigen presentation to establish persistent infection. In contrast, autophagy is known to serve as a negative regulator of innate immunity (21, 54). A recent report demonstrated that autophagy induced by infection with strain JFH1 or dengue virus attenuates innate immunity to promote viral replication (23), indicating that an HCV genotype 2a strain may facilitate autophagy to evade innate immunity.

In this study, we demonstrated that HCV utilizes autophagy to circumvent the cell death induced by vacuole formation for its survival. This unique strategy of HCV propagation may provide new clues to the virus-host interaction and, ultimately, to the pathogenesis of infection by various genotypes of HCV.

ACKNOWLEDGMENTS

We thank H. Murase and M. Tomiyama for their secretarial work. We also thank R. Bartenschlager and T. Wakita for providing cell lines and plasmids.

This work was supported in part by grants-in-aid from the Ministry of Health, Labor, and Welfare (Research on Hepatitis), the Ministry of Education, Culture, Sports, Science, and Technology, and the Osaka University Global Center of Excellence Program.

REFERENCES

1. **Auffermann-Gretzinger, S., E. B. Keeffe, and S. Levy.** 2001. Impaired dendritic cell maturation in patients with chronic, but not resolved, hepatitis C virus infection. Blood **97:**3171–3176.
2. **Beyenbach, K. W., and H. Wieczorek.** 2006. The V-type H+ ATPase: molecular structure and function, physiological roles and regulation. J. Exp. Biol. **209:**577–589.
3. **Bradley, D. W.** 2000. Studies of non-A, non-B hepatitis and characterization of the hepatitis C virus in chimpanzees. Curr. Top. Microbiol. Immunol. **242:**1–23.
4. **Clarke, P. G.** 1990. Developmental cell death: morphological diversity and multiple mechanisms. Anat. Embryol. (Berl.) **181:**195–213.
5. **Dreux, M., P. Gastaminza, S. F. Wieland, and F. V. Chisari.** 2009. The autophagy machinery is required to initiate hepatitis C virus replication. Proc. Natl. Acad. Sci. U. S. A. **106:**14046–14051.
6. **English, L., et al.** 2009. Autophagy enhances the presentation of endogenous viral antigens on MHC class I molecules during HSV-1 infection. Nat. Immunol. **10:**480–487.
7. **Fujita, N., et al.** 2008. An Atg4B mutant hampers the lipidation of LC3 paralogues and causes defects in autophagosome closure. Mol. Biol. Cell **19:**4651–4659.
8. **Fujita, N., et al.** 2008. The Atg16L complex specifies the site of LC3 lipidation for membrane biogenesis in autophagy. Mol. Biol. Cell **19:**2092–2100.
9. **Fujitani, Y., C. Ebato, T. Uchida, R. Kawamori, and H. Watada.** 2009. β-cell autophagy: a novel mechanism regulating β-cell function and mass: lessons from β-cell-specific Atg7-deficient mice. Islets **1:**151–153.
10. **Gannage, M., et al.** 2009. Matrix protein 2 of influenza A virus blocks autophagosome fusion with lysosomes. Cell Host Microbe **6:**367–380.
11. **Gannage, M., and C. Munz.** 2009. Autophagy in MHC class II presentation of endogenous antigens. Curr. Top. Microbiol. Immunol. **335:**123–140.
12. **Hara, T., et al.** 2006. Suppression of basal autophagy in neural cells causes neurodegenerative disease in mice. Nature **441:**885–889.
13. **Hasilik, A.** 1992. The early and late processing of lysosomal enzymes: proteolysis and compartmentation. Experientia **48:**130–151.

14. **Hatzakis, A., et al.** 1996. Hepatitis C virus 1b is the dominant genotype in HCV-related carcinogenesis: a case-control study. Int. J. Cancer **68:**51–53.
15. **Hirabayashi, M., et al.** 2001. VCP/p97 in abnormal protein aggregates, cytoplasmic vacuoles, and cell death, phenotypes relevant to neurodegeneration. Cell Death Differ. **8:**977–984.
16. **Hiraga, N., et al.** 2011. Rapid emergence of telaprevir resistant hepatitis C virus strain from wildtype clone in vivo. Hepatology (Baltimore, Md.) **54:** 781–788.
17. **Hiraga, N., et al.** 2007. Infection of human hepatocyte chimeric mouse with genetically engineered hepatitis C virus and its susceptibility to interferon. FEBS Lett. **581:**1983–1987.
18. **Ichimura, Y., E. Kominami, K. Tanaka, and M. Komatsu.** 2008. Selective turnover of p62/A170/SQSTM1 by autophagy. Autophagy **4:**1063–1066.
19. **Isidoro, C., et al.** 1995. Altered intracellular processing and enhanced secretion of procathepsin D in a highly deviated rat hepatoma. Int. J. Cancer **60:**61–64.
20. **Jacobson, I. M., P. Cacoub, L. Dal Maso, S. A. Harrison, and Z. M. Younossi.** 2010. Manifestations of chronic hepatitis C virus infection beyond the liver. Clin. Gastroenterol. Hepatol. **8:**1017–1029.
21. **Jounai, N., et al.** 2007. The Atg5 Atg12 conjugate associates with innate antiviral immune responses. Proc. Natl. Acad. Sci. U. S. A. **104:**14050–14055.
22. **Kanto, T., et al.** 1999. Impaired allostimulatory capacity of peripheral blood dendritic cells recovered from hepatitis C virus-infected individuals. J. Immunol. **162:**5584–5591.
23. **Ke, P. Y., and S. S. Chen.** 2011. Activation of the unfolded protein response and autophagy after hepatitis C virus infection suppresses innate antiviral immunity in vitro. J. Clin. Invest. **121:**37–56.
24. **Kimura, S., N. Fujita, T. Noda, and T. Yoshimori.** 2009. Monitoring autophagy in mammalian cultured cells through the dynamics of LC3. Methods Enzymol. **452:**1–12.
25. **Kiyosawa, K., et al.** 1990. Interrelationship of blood transfusion, non-A, non-B hepatitis and hepatocellular carcinoma: analysis by detection of antibody to hepatitis C virus. Hepatology **12:**671–675.
26. **Koblinski, J. E., et al.** 2002. Interaction of human breast fibroblasts with collagen I increases secretion of procathepsin B. J. Biol. Chem. **277:**32220–32227.
27. **Koike, K., et al.** 1997. Sialadenitis histologically resembling Sjogren syndrome in mice transgenic for hepatitis C virus envelope genes. Proc. Natl. Acad. Sci. U. S. A. **94:**233–236.
28. **Koike, K., T. Tsutsumi, H. Yotsuyanagi, and K. Moriya.** 2010. Lipid metabolism and liver disease in hepatitis C viral infection. Oncology **78**(Suppl. 1)**:**24–30.
29. **Komatsu, M., et al.** 2006. Loss of autophagy in the central nervous system causes neurodegeneration in mice. Nature **441:**880–884.
30. **Komatsu, M., et al.** 2007. Homeostatic levels of p62 control cytoplasmic inclusion body formation in autophagy-deficient mice. Cell **131:**1149–1163.
31. **Lee, J. H., et al.** 2010. Lysosomal proteolysis and autophagy require presenilin 1 and are disrupted by Alzheimer-related PS1 mutations. Cell **141:** 1146–1158.
32. **Levine, B., and G. Kroemer.** 2008. Autophagy in the pathogenesis of disease. Cell **132:**27–42.
33. **Lindenbach, B. D., et al.** 2005. Complete replication of hepatitis C virus in cell culture. Science **309:**623–626.
34. **Lohmann, V., et al.** 1999. Replication of subgenomic hepatitis C virus RNAs in a hepatoma cell line. Science **285:**110–113.
35. **Manns, M. P., et al.** 2001. Peginterferon alfa-2b plus ribavirin compared with interferon alfa-2b plus ribavirin for initial treatment of chronic hepatitis C: a randomised trial. Lancet **358:**958–965.
36. **McHutchison, J. G., et al.** 2009. Telaprevir with peginterferon and ribavirin for chronic HCV genotype 1 infection. N. Engl. J. Med. **360:**1827–1838.
37. **Mizushima, N.** 2007. Autophagy: process and function. Genes Dev. **21:**2861–2873.
38. **Moradpour, D., F. Penin, and C. M. Rice.** 2007. Replication of hepatitis C virus. Nat. Rev. Microbiol. **5:**453–463.
39. **Moriishi, K., and Y. Matsuura.** 2007. Host factors involved in the replication of hepatitis C virus. Rev. Med. Virol. **17:**343–354.
40. **Moriishi, K., and Y. Matsuura.** 2003. Mechanisms of hepatitis C virus infection. Antivir. Chem. Chemother. **14:**285–297.
41. **Oda, K., Y. Nishimura, Y. Ikehara, and K. Kato.** 1991. Bafilomycin A1 inhibits the targeting of lysosomal acid hydrolases in cultured hepatocytes. Biochem. Biophys. Res. Commun. **178:**369–377.
42. **Orvedahl, A., et al.** 2007. HSV-1 ICP34.5 confers neurovirulence by targeting the Beclin 1 autophagy protein. Cell Host Microbe **1:**23–35.
43. **Poordad, F., et al.** 2011. Boceprevir for untreated chronic HCV genotype 1 infection. N. Engl. J. Med. **364:**1195–1206.
44. **Pua, H. H., I. Dzhagalov, M. Chuck, N. Mizushima, and Y. W. He.** 2007. A critical role for the autophagy gene Atg5 in T cell survival and proliferation. J. Exp. Med. **204:**25–31.
45. **Ramachandran, N., et al.** 2009. VMA21 deficiency causes an autophagic myopathy by compromising V-ATPase activity and lysosomal acidification. Cell **137:**235–246.
46. **Saito, K., et al.** 2008. Hepatitis C virus inhibits cell surface expression of HLA-DR, prevents dendritic cell maturation, and induces interleukin-10 production. J. Virol. **82:**3320–3328.
47. **Schmid, D., and C. Munz.** 2007. Innate and adaptive immunity through autophagy. Immunity **27:**11–21.
48. **Schutte, K., J. Bornschein, and P. Malfertheiner.** 2009. Hepatocellular carcinoma—epidemiological trends and risk factors. Dig. Dis. **27:**80–92.
49. **Sir, D., et al.** 2008. Induction of incomplete autophagic response by hepatitis C virus via the unfolded protein response. Hepatology **48:**1054–1061.
50. **Sloane, B. F., et al.** 2005. Cathepsin B and tumor proteolysis: contribution of the tumor microenvironment. Semin. Cancer Biol. **15:**149–157.
51. **Stankovic-Djordjevic, D., et al.** 2007. Hepatitis C virus genotypes and the development of hepatocellular carcinoma. J. Dig. Dis. **8:**42–47.
52. **Strader, D. B., T. Wright, D. L. Thomas, and L. B. Seeff.** 2004. Diagnosis, management, and treatment of hepatitis C. Hepatology **39:**1147–1171.
53. **Taguwa, S., et al.** 2009. Cochaperone activity of human butyrate-induced transcript 1 facilitates hepatitis C virus replication through an Hsp90-dependent pathway. J. Virol. **83:**10427–10436.
54. **Tal, M. C., et al.** 2009. Absence of autophagy results in reactive oxygen species-dependent amplification of RLR signaling. Proc. Natl. Acad. Sci. U. S. A. **106:**2770–2775.
55. **Tardif, K. D., and A. Siddiqui.** 2003. Cell surface expression of major histocompatibility complex class I molecules is reduced in hepatitis C virus subgenomic replicon-expressing cells. J. Virol. **77:**11644–11650.
56. **Wakita, T., et al.** 2005. Production of infectious hepatitis C virus in tissue culture from a cloned viral genome. Nat. Med. **11:**791–796.
57. **Walker, C. M.** 1997. Comparative features of hepatitis C virus infection in humans and chimpanzees. Springer Semin. Immunopathol. **19:**85–98.
58. **Wasley, A., and M. J. Alter.** 2000. Epidemiology of hepatitis C: geographic differences and temporal trends. Semin. Liver Dis. **20:**1–16.
59. **Wong, J., et al.** 2008. Autophagosome supports coxsackievirus B3 replication in host cells. J. Virol. **82:**9143–9153.
60. **Yoshimori, T., and T. Noda.** 2008. Toward unraveling membrane biogenesis in mammalian autophagy. Curr. Opin. Cell Biol. **20:**401–407.

Published OnlineFirst August 29, 2011; DOI:10.1158/1055-9965.EPI-11-0464

Cancer Epidemiology, Biomarkers & Prevention

Research Article

Prediction of Hepatocellular Carcinoma Development by Plasma ADAMTS13 in Chronic Hepatitis B and C

Hitoshi Ikeda[1,2], Ryosuke Tateishi[2], Kenichiro Enooku[1,2], Haruhiko Yoshida[2], Hayato Nakagawa[1,2], Ryota Masuzaki[2], Yuji Kondo[2], Tadashi Goto[2], Shuichiro Shiina[2], Yukio Kume[1], Tomoaki Tomiya[2], Yukiko Inoue[2], Takako Nishikawa[2], Natsuko Ohtomo[2], Yasushi Tanoue[2], Tomoko Ono[3], Kazuhiko Koike[2], and Yutaka Yatomi[1]

Abstract

Background: Chronic liver injury evokes a wound healing response, promoting fibrosis and finally hepatocellular carcinoma (HCC), in which hepatic stellate cells play an important role. Although a blood marker of hepatic stellate cells is not known, those cells importantly contribute to the regulation of plasma a disintegrin-like and metalloproteinase with thrombospondin type-1 motifs 13 (ADAMTS13) activity, a defect of which causes thrombotic thrombocytopenic purpura.

Methods: Plasma ADAMTS13 was evaluated in chronic hepatitis B or C patients with or without HCC.

Results: Plasma ADAMTS13 activity significantly correlated with serum aspartate aminotransferase and alanine aminotransferase, liver stiffness value, and aspartate aminotransferase-to-platelet ratio index, irrespective of the presence of HCC, suggesting that it may reflect hepatocellular damage and subsequent wound healing and fibrosis as a result of hepatic stellate cell action. During the three-year follow-up period for patients without HCC, it developed in 10 among 81 patients. Plasma ADAMTS13 activity was significantly higher in patients with HCC development than in those without and was a significant risk for HCC development by univariate and multivariate analyses. Furthermore, during the one-year follow-up period for patients with HCC treated with radiofrequency ablation, HCC recurred in 55 among 107 patients. Plasma ADAMTS13 activity or antigen level was significantly higher in patients with HCC recurrence than in those without and was retained as a significant risk for HCC recurrence by multivariate analysis.

Conclusions: Higher plasma ADAMTS13 activity and antigen level was a risk of HCC development in chronic liver disease.

Impact: Plasma ADAMTS13 as a potential marker of hepatic stellate cells may be useful in the prediction of hepatocarcinogenesis. *Cancer Epidemiol Biomarkers Prev; 20(10); 2204–11. ©2011 AACR.*

Introduction

It is well known that chronic wound healing generally provides a microenvironment that gives rise to cancer (1). Indeed, chronic injury in the liver evokes a perpetuating wound healing response, promoting the development of fibrosis and finally hepatocellular carcinoma (HCC; ref. 2). Among the cells in the liver, hepatic stellate cells are known as a main effector of wound healing and fibrosis following liver injury of any etiology (3), however, a useful blood marker to reflect the activity of those cells has not been found yet in the clinical setting.

In this context, we have focused on a disintegrin-like and metalloproteinase with thrombospondin type-1 motifs 13 (ADAMTS13), a defect of which increases unusually large multimers of von Willebrand factor in the plasma, causes platelet thrombosis under high sheer stress, and results finally in thrombotic thrombocytopenic purpura (4–6). With regard to the site of production, *ADAMTS13* mRNA expression was shown exclusively in the liver (7–9) and then both *ADAMTS13* mRNA expression and ADAMTS13 activity were determined primarily in hepatic stellate cells among the liver cells in mice (10). ADAMTS13 expression was also detected in hepatic stellate cells in human and thereby ADAMTS13 is reportedly produced in those cells (11). To elucidate a regulatory mechanism of plasma ADAMTS13 activity, we previously determined that selective hepatic stellate cell damage caused by dimethylnitrosamine in rats leads to decreased plasma ADAMTS13 activity (12). On the other hand, plasma ADAMTS13 activity was upregulated during the process of liver fibrosis due to cholestasis caused by bile duct ligation and steatohepatitis induced by a choline-deficient L-amino acid–defined diet in rats, in which hepatic stellate cells actively proliferate (13).

Authors' Affiliations: Departments of [1]Clinical Laboratory Medicine and [2]Gastroenterology, Graduate School of Medicine, The University of Tokyo, Hongo, Bunkyo-ku, Tokyo; and [3]Mitsubishi Chemical Medicine Corporation, Ohwadashinden, Yachiyo-shi Chiba, Japan

Corresponding Author: Hitoshi Ikeda, Department of Clinical Laboratory Medicine, Graduate School of Medicine, The University of Tokyo, 7-3-1 Hongo, Bunkyo-ku, Tokyo 113-8655, Japan. Phone: 81-3-3815-5411; Fax: 81-3-5689-0495; E-mail: ikeda-1im@h.u-tokyo.ac.jp

doi: 10.1158/1055-9965.EPI-11-0464

Published OnlineFirst August 29, 2011; DOI:10.1158/1055-9965.EPI-11-0464

These results indicate that hepatic stellate cells play an important role in the regulation of plasma ADAMTS13 activity, although other sources of ADAMTS13 were reported (14–16).

On the basis of these previous findings, we wondered whether plasma ADAMTS13 could be a blood marker of hepatic stellate cells. To examine this, plasma ADAMTS13 was evaluated in patients with chronic hepatitis B or C, in whom chronic wound healing and fibrosis are observed with a high risk of HCC development (17), in which hepatic stellate cells play an important role (3). In this study, we have found that plasma ADAMTS13 was increased in relation with serum levels of aspartate aminotransferase (AST) or alanine aminotransferase (ALT), and the markers of liver fibrosis and that higher plasma ADAMTS13 was more frequently found in patients who later developed HCC.

Patients and Methods

Patients

Eighty-one patients with chronic hepatitis B and C, who visited the Department of Gastroenterology, the University of Tokyo Hospital, Tokyo, Japan, between April and August in 2007, were first enrolled. Chronic hepatitis B was defined as hepatitis B surface antigen (HBsAg) positivity, and chronic hepatitis C was defined as serum anti-hepatitis C virus antibody (HCVAb) positivity and a detectable HCV RNA level, having persistent liver damage for more than 6 months. Patients with HCC at the time of enrollment or with past history of HCC were excluded from this analysis.

Next, between July and September in 2009, 107 consecutive patients with chronic hepatitis B and C with HCC who were scheduled to undergo radiofrequency ablation (RFA) for HCC were enrolled.

All the studies were carried out in accordance with the ethical guidelines of the 1975 Declaration of Helsinki and were approved by the Institutional Research Ethics Committee of the Faculty of Medicine of the University of Tokyo. Informed consent from the patients was obtained for the use of the samples in this study.

Measurement of ADAMTS13 activity

ADAMTS13 enzymatic activity was measured manually using a chromogenic ELISA kit, ADAMTS13-act-ELISA (Kainos Inc./Technoclone GmbH), which captures products cleaved by ADAMTS13 using a sandwich method, and expressed as percentage of healthy control. The very high correlation of the values measured by classical VWF multimer assay and this novel chromogenic ADAMTS13-act-ELISA was reported previously (18).

Measurement of ADAMTS13 antigen level

ADAMTS13 antigen level was measured by a latex photometric immunoassay, in which suspended polystyrene latex particles coated with polyclonal antibody F(ab')2 fragment against ADAMTS13 were employed. Antisera against ADAMTS13 were obtained by immunization with pCAG-ADAMTS13 plasmid DNA (donated by Dr. Soejima from The Chemo-Sero-Therapeutic Research Institute, Kumamoto, Japan) using electroporation. Latex agglutination was analyzed using LPIA-A700 (Mitsubishi Chemical Medience Co.), a fully automated quantitative latex photometric immunoassay instrument. ADAMTS13 antigen level in sample of each patient was expressed as the percentage of that in pooled normal human plasma.

Measurement of liver stiffness

Liver stiffness was measured by transient elastography (FibroScan 502; EchoSens) as described previously (19–21). Briefly, the measurements were done in the right lobe of the liver through the intercostal spaces, with the patient lying in the dorsal decubitus position, and were considered valid only when at least 10 acquisitions were successful, with a success rate of at least 60% and the ratio of interquartile range to the median value was larger than 30%. Liver stiffness value was expressed in kilopascals (kPa).

Patient follow-up and diagnosis of HCC

Patients without HCC were followed up at the outpatient clinic with monthly blood tests, including tumor markers and ultrasonography every 4 to 6 months. Contrast-enhanced computed tomography (CT) was done when serum alpha-fetoprotein (AFP) levels and/or plasma des-gamma-carboxy prothrombin (DCP) levels showed an abnormal rise and/or tumors were detected as possible HCC on ultrasonography. The diagnosis of HCC was based on typical findings on CT, that is, hyperattenuation in the arterial phase and hypoattenuation in the equilibrium phase (22–24).

The end points consisted of the interval between the first measurement of plasma ADAMTS13 activity and the detection of HCC development, death without HCC development, or the last examination until 30 July 2010, whichever came first. Death without HCC development was treated as censored data.

Radiofrequency ablation, patient follow-up, and analysis of HCC recurrence

The detailed procedure of RFA was meticulously described elsewhere (25). The indication criteria for RFA consisted of total bilirubin concentration less than 3.0 mg/dL and platelet count more than $5 \times 10^4/\mu L$. Patients with portal vein tumor thrombosis, massive refractory ascites, or extrahepatic metastasis were excluded. In general, RFA was done on patients with 3 or fewer lesions, each less than 3.0 cm in diameter. However, RFA was also done on patients who did not meet these criteria when complete ablation could be anticipated in all tumors without deteriorating liver function. After RFA, dynamic CT was done to evaluate treatment efficacy. Complete ablation was defined as hypoattenuation of the whole lesion together with the surrounding liver parenchyma as a safety margin.

Published OnlineFirst August 29, 2011; DOI:10.1158/1055-9965.EPI-11-0464

Patients received additional RFA until complete ablation was confirmed for each HCC nodule.

The follow-up consisted of monthly blood tests and monitoring of tumor markers at the outpatient clinic, with ultrasonography and dynamic CT scan done every 4 months. HCC recurrence was diagnosed on the basis of the criteria as described earlier.

The end points consisted of the interval between the first ablation and the detection of HCC recurrence, death without recurrence, or the last examination until 30 September 2010, whichever came first. Death without recurrence was treated as censored data.

Statistical analysis

Comparisons between groups were made using Student's t test or χ^2 test. The correlation between 2 groups, in which the data points were distribution free, was analyzed using Spearman's rank correlation coefficient (ρs). The cumulative incidence of HCC was estimated using the Kaplan–Meier method. In the analysis of risk factors for hepatocarcinogenesis, we tested the following variables obtained at the time of entry in univariate and multivariate Cox proportional hazard regression analyses: age, sex, positivity for HBsAg and HCVAb, albumin, total bilirubin, AST, ALT, prothrombin time, platelet counts, liver stiffness value, APRI, AFP, DCP, and either plasma ADAMTS13 activity or antigen level. Multichotomous categorical variables were represented by corresponding binary dummy variables. Factors that had a $P < 0.2$ in univariate analysis were subsequently included in a multivariate Cox proportional hazard regression model, with stepwise selection of variables based on the Akaike information criterion (AIC). Data processing and analysis were done by using the S-plus Ver. 7 (TIBCO Software Inc.).

Results

Characteristics of the patients without HCC and correlation between plasma ADAMTS13 activity and clinical variables

The characteristics of the patients, who were first enrolled for the measurement of plasma ADAMTS13 activity, are summarized in Table 1. There were 21 patients with chronic hepatitis B and 60 patients with chronic hepatitis C. All the patients were outpatients without HCC at the time of enrollment and past history of HCC.

Plasma ADAMTS13 activity in these patients was 114.0 ± 45.4% (mean ± SD) of control, ranged from 28.0% to 221.5%, as shown in Table 1. Relationships between plasma ADAMTS13 activity and clinical variables are shown in Table 2. The significant correlations were determined between plasma ADAMTS13 activity and serum AST and ALT levels ($P < 0.001$). On the other hand, the significant correlations were also determined between plasma ADAMTS13 activity and the variables predicting the stage of liver fibrosis, liver stiffness value ($P < 0.001$), and aspartate aminotransferase-to-platelet ratio index (APRI; $P = 0.027$). Of note is the finding that plasma ADAMTS13 activity significantly correlated with serum AFP level ($P < 0.001$).

HCC development and risk analysis

Next, a potential link between plasma ADAMTS13 activity and HCC was examined. During the mean follow-up period of 35.4 months, one patient had been lost to follow-up evaluation and one patient died before HCC was identified. By the end of the follow-up, HCC developed in 10 patients, among whom 2 patients died of HCC. The cumulative incidence rates of HCC at

Table 1. Characteristics of patients without HCC or with HCC

Variables	Patients without HCC	Patients with HCC
Age (y)	63 ± 12 (23–85)	68.9 ± 8.5 (43–86)
Man/Woman	49/32	68/39
HBV/HCV	21/60	15/92
Albumin (g/dL)	4.1 ± 0.4 (3.1–4.9)	3.7 ± 0.6 (2.0–5.1)
AST (U/L)	48 ± 35 (3–270)	61.4 ± 39.2 (16–289)
ALT (U/L)	53 ± 66 (11–542)	54.1 ± 38.6 (11–276)
Platelet count (× 10^4/μL)	15.2 ± 6.3 (3.4–30.8)	10.8 ± 4.7 (3.4–25.2)
Prothrombin time (%)	87.7 ± 11.6 (49.2–100.0)	98.3 ± 5.2 (73.0–100.0)
Plasma ADAMTS13 activity (%)	114.0 ± 45.4 (28.0–221.5)	125.0 ± 32.4 (62.0–223.0)
Plasma ADAMTS13 antigen level (%)	Not measured	128.6 ± 39.6 (48.9–258.3)
Liver stiffness (kPa)	11.4 ± 9.2 (3.1–48.0)	28.5 ± 17.9 (6.1–75.0)
APRI	1.07 ± 1.00 (0.08–5.92)	1.89 ± 1.44 (0.22–7.81)
AFP (ng/mL)	12.6 ± 38.2 (1–319)	99.4 ± 361.2 (1–3,399)
DCP (mAu/mL)	18.1 ± 17.6 (10–165)	70.7 ± 194.3 (8–1,462)
Maximum size of HCC (mm)	Not available	17.8 ± 6.0 (6.0–33.0)

NOTE: Values are expressed as the mean ± SD (range).

Published OnlineFirst August 29, 2011; DOI:10.1158/1055-9965.EPI-11-0464

Table 2. Relation between plasma ADAMTS13 activity and clinical variables in patients without HCC or with HCC

Variables	Patients without HCC		Patients with HCC	
	ρs[a]	*P*	ρs[a]	*P*
Age	−0.067	0.554	−0.030	0.760
AST (U/L)	0.360	<0.001	0.531	<0.001
ALT (U/L)	0.426	<0.001	0.519	<0.001
Albumin (g/dL)	−0.114	0.309	−0.146	0.133
Platelet count (× 10^4/μL)	−0.091	0.418	−0.129	0.185
Prothrombin time (%)	−0.343	<0.005	−0.029	0.764
Liver stiffness (kPa)	0.379	<0.001	0.216	0.026
APRI	0.245	0.027	0.403	<0.001
AFP (ng/mL)	0.465	<0.001	0.554	<0.001
DCP (mAu/mL)	0.135	0.230	−0.281	0.003
Size of HCC (mm)[b]	Not available		−0.075	0.571

[a]Spearman's rank correlation coefficient.
[b]Analyzed in patients with single nodule of HCC.

1, 2, and 3 years estimated by the Kaplan–Meier method were 4.9%, 9.1%, and 11.1%, respectively, as shown in Figure 1A. In these patients who developed HCC, plasma ADAMTS13 activity was significantly higher than that in patients who did not develop HCC ($P < 0.001$), as depicted in Table 3; plasma ADAMTS13 activity was 161.9 ± 33.8% in patients who developed HCC and 108.8 ± 42.2% in patients who did not develop HCC. Liver stiffness value was also significantly higher in patients with HCC development, and serum albumin level and prothrombin time (%) were significantly lower in those patients. Then, univariate analyses showed that the higher plasma ADAMTS13 activity was a risk for HCC development ($P < 0.001$; Table 4). Other significant risk factors for HCC included lower albumin level, higher ALT level, lower prothrombin time (%), and higher liver stiffness value. Next, stepwise variable selection with AIC was used to find the best model in multivariate analysis (Table 4), which revealed that the higher plasma ADAMTS13 activity ($P = 0.03$) and the higher liver stiffness value ($P = 0.03$) were the significant risk factors for HCC. These results suggest that plasma ADAMTS13 activity may predict HCC development in patients with chronic hepatitis B or C.

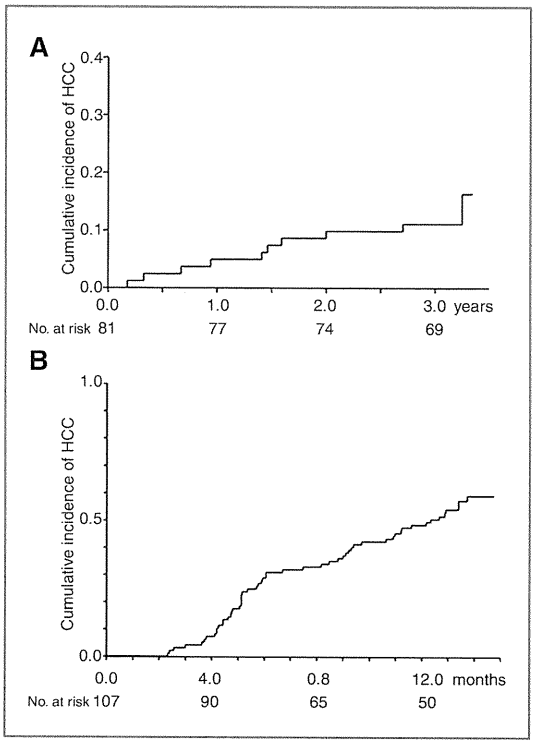

Figure 1. Cumulative incidence of HCC development (A) and recurrence (B).

Then, the relation between plasma ADAMTS13 activity and HCC development was analyzed separately in patients with chronic hepatitis B and with chronic hepatitis C. In patients with chronic hepatitis B ($n = 20$), plasma ADAMTS13 activity was significantly higher in patients who developed HCC than that in patients who did not develop HCC ($P < 0.005$); plasma ADAMTS13 activity was 158.9 ± 36.7% in patients who developed HCC and 95.3 ± 35.0% in patients who did not develop HCC. Then, univariate analyses showed that the higher plasma ADAMTS13 activity was a risk for HCC development ($P < 0.001$), and further multivariate analysis revealed that the higher plasma ADAMTS13 activity was a significant risk factor for HCC ($P = 0.03$) in these patients. In patients

Published OnlineFirst August 29, 2011; DOI:10.1158/1055-9965.EPI-11-0464

Table 3. Characteristics of patients according to HCC development and recurrence

Variables	Development (−)	Development (+)	*P*	Recurrence (−)	Recurrence (+)	*P*
Age (y)	63.0 ± 12.4	61.4 ± 12.4	0.695	70.2 ± 7.5	68.3 ± 9.2	0.267
Man/Woman	40/29	6/4	0.82	23/19	36/19	0.39
HBV/HCV	16/53	4/6	0.45	7/35	7/48	0.80
Albumin (g/dL)	4.1 ± 0.3	3.8 ± 0.6	0.024	3.8 ± 0.5	3.6 ± 0.6	0.296
AST (IU/L)	46.9 ± 36.6	55.1 ± 23.0	0.494	61.0 ± 46.5	60.5 ± 33.3	0.951
ALT (IU/L)	52.0 ± 68.8	63.2 ± 46.9	0.620	56.9 ± 46.7	49.7 ± 29.5	0.359
Platelet count ($\times 10^4/\mu L$)	15.7 ± 6.5	12.2 ± 3.9	0.097	10.9 ± 5.5	10.5 ± 4.3	0.667
Prothrombin time (%)	89.5 ± 10.5	74.7 ± 11.6	<0.001	98.9 ± 3.5	97.5 ± 6.5	0.188
Plasma ADAMTS13 activity (%)	108.8 ± 42.2	161.9 ± 33.8	<0.001	116.8 ± 28.5	130.0 ± 30.8	0.039
Plasma ADAMTS13 antigen (%)	Not measured	Not measured		118.9 ± 35.4	134.3 ± 36.1	0.037
Liver stiffness (kPa)	9.2 ± 5.7	22.6 ± 13.7	<0.001	23.4 ± 15.0	30.6 ± 18.4	0.053
APRI	1.03 ± 1.03	1.35 ± 0.80	0.35	1.57 ± 0.81	1.47 ± 0.77	0.517
AFP (ng/mL)	10.7 ± 38.1	27.4 ± 41.4	0.203	131.5 ± 546.0	81.2 ± 158.1	0.521
DCP (mAu/mL)	17.9 ± 18.8	19.7 ± 8.2	0.766	114.0 ± 297.6	41.7 ± 64.3	0.082

NOTE: Values are expressed as the mean ± SD (range).

with chronic hepatitis C ($n = 59$), plasma ADAMTS13 activity was significantly higher in patients who develop HCC than that in patients who did not develop HCC ($P < 0.01$); plasma ADAMTS13 activity was 163.9 ± 35.2% in patients who developed HCC and 112.9 ± 43.6% in patients who did not develop HCC. Then, univariate analyses showed that the higher plasma ADAMTS13 activity was a risk for HCC development ($P < 0.001$), and multivariate analysis revealed that the higher plasma ADAMTS13 activity was a significant risk factor for HCC ($P = 0.02$) in these patients.

Characteristics of the patients with HCC and correlation between plasma ADAMTS13 activity or antigen level and clinical variables

To further examine a potential link between plasma ADAMTS13 and HCC, plasma ADAMTS13 activity and antigen level were measured in 107 patients with HCC. Their characteristics are summarized in Table 1. There were 15 patients with chronic hepatitis B and 92 patients with chronic hepatitis C.

Plasma ADAMTS13 activity in these patients was 124.9% ± 32.3% (mean ± SD) of control, ranged from 62.0% to 223.0%, and plasma ADAMTS13 antigen level, 128.3% ± 39.3% (mean ± SD) of control, ranged from 48.9% to 258.3%, respectively (Table 1). Of note, the strong correlation between plasma ADAMTS13 activity and plasma ADAMTS13 antigen level was observed (Spearman's rank; $\rho s = 0.803$, $P < 0.00001$, $n = 107$). Relationships between plasma ADAMTS13 activity and clinical variables are shown in Table 2. Same as in patients without HCC, the significant correlations were determined between plasma ADAMTS13 activity and serum AST and ALT levels ($P < 0.001$), liver stiffness value ($P = 0.026$), APRI ($P < 0.001$), and serum AFP level ($P < 0.001$). Of note, there was no significant correlation between plasma ADAMTS13 activity and maximum tumor size in patients with single nodule, suggesting that plasma ADAMTS13 activity is not a tumor marker of HCC.

Table 4. Risk factors for HCC development–univariate and multivariate analyses

Variable	HR (95% CI)	*P*
Univariate analysis		
ADAMTS13 (per 10% increase)	1.29 (1.11–1.50)	<0.001
Age (per 1 year increase)	0.990 (0.943–1.04)	0.68
Sex (male vs. female)	1.07 (0.563–2.02)	0.84
Hepatitis virus (HCV vs. HBV)	0.718 (0.380–1.36)	0.31
Albumin (per 1 g/dL increase)	0.208 (0.0477–0.905)	0.04
AST >40 U/L	1.73 (0.881–3.41)	0.11
ALT >40 U/L	2.06 (1.05–4.07)	0.04
PLT $<15 \times 10^4/\mu L$	1.97 (0.908–4.29)	0.09
Prothrombin time (%; per 10% increase)	0.490 (0.324–0.743)	<0.001
Liver stiffness (per 10% increase)	1.16 (1.07–1.26)	<0.001
APRI (per 10% increase)	1.05 (0.983–1.13)	0.14
AFP >20 ng/mL	1.71 (0.785–3.71)	0.18
DCP >40 mAU/mL[a]	NA	
Multivariate analysis		
ADAMTS13 (per 10% increase)	1.20 (1.02–1.40)	0.03
Liver stiffness (per 10% increase)	1.12 (1.01–1.23)	0.03

[a]Not accessed as only DCP was more than 40 mAU/mL in only 1 patient.

Published OnlineFirst August 29, 2011; DOI:10.1158/1055-9965.EPI-11-0464

HCC recurrence and risk analysis

During the follow-up period of 12 months, 1 patient died without HCC. Two patients who developed extrahepatic recurrence and 3 patients who developed recurrence at a site adjacent to the treated site were excluded from the analysis. Four patients who were treated with IFN were not analyzed because IFN is known to reduce the risk of HCC development in chronic hepatitis B and C (26, 27). By the end of the follow-up, HCC recurrence was determined in 55 patients. The cumulative recurrence rates of HCC by the Kaplan–Meier method are shown in Figure 1B. The characteristics of patients with or without HCC recurrence are shown in Table 3. Among the various parameters, plasma ADAMTS13 activity ($P = 0.039$) and antigen level ($P = 0.037$) were significantly higher in patients with HCC recurrence than those in patients without HCC recurrence (Table 3). No significant differences were determined in other parameters between patients with and without HCC recurrence. Although there was no significant risk factor for HCC recurrence in univariate analyses (Table 5), plasma ADAMTS13 activity was retained as a significant risk factor of HCC recurrence ($P = 0.028$) in the multivariate Cox proportional hazard model, as shown in Table 5. When plasma ADAMTS13 antigen level was analyzed instead of plasma ADAMTS13 activity level, plasma ADAMTS13 antigen level was also a significant risk factor of HCC recurrence ($P = 0.007$) in multivariate analysis. These results suggest that plasma ADAMTS13 activity may predict HCC recurrence in patients with chronic hepatitis B or C.

Table 5. Risk factors for HCC recurrence–univariate and multivariate analyses

Variable	HR (95%CI)	P
Univariate analysis		
ADAMTS13 activity (per 10% increase)	1.106 (0.997–1.228)	0.052
Age (per 1 year increase)	0.982 (0.953–1.013)	0.25
Sex (male vs. female)	1.22 (0.70–2.13)	0.49
Hepatitis virus (HCV vs. HBV)	1.10 (0.50–2.44)	0.81
Albumin (per 1g/dL increase)	0.723 (0.432–1.210)	0.22
AST > 40 IU/L	1.35 (0.75–2.42)	0.31
ALT > 40 IU/L	1.00 (0.58–1.71)	0.99
PLT < 15 × 10^4/μL	1.25 (0.65–2.43)	0.51
Prothrombin Activity (per 10% increase)	0.88 (0.42–1.07)	0.20
Liver stiffness (per 10% increase)	1.12 (0.98–1.28)	0.11
APRI (per 10% increase)	1.00 (0.973–1.04)	0.81
AFP > 20 ng/mL	1.24 (0.73–2.11)	0.42
DCP > 40 mAU/mL	1.17 (0.64–2.14)	0.62
Multivariate analysis		
ADAMTS13 activity (per 10% increase)	1.14 (1.01–1.29)	0.028

The relation between plasma ADAMTS13 activity and HCC recurrence was also analyzed separately in patients with chronic hepatitis B and with chronic hepatitis C. In patients with chronic hepatitis B ($n = 14$), plasma ADAMTS13 activity or antigen level was not different between patients with (105.0 ± 34.0% or 97.3 ± 24.7%) and without HCC recurrence (104.0 ± 16.3% or 98.9 ± 14.4%), possibly because the number of patients analyzed was small. On the other hand, in patients with chronic hepatitis C ($n = 83$), plasma ADAMTS13 activity or antigen level was significantly higher in patients with HCC recurrence (133.2 ± 28.9% or 139.7 ± 34.4%) than that in patients without HCC recurrence (119.4 ± 29.8% or 122.9 ± 37.1; $P = 0.037$ or $P = 0.036$). Multivariate analysis revealed that the higher plasma ADAMTS13 activity or antigen level was a significant risk factor for HCC ($P = 0.024$ or $P = 0.005$) in these patients.

Discussion

In the current study, plasma ADAMTS13 activity or antigen level significantly correlated with serum AST and ALT levels and also the variables predicting the stage of liver fibrosis, liver stiffness value, and APRI in patients with chronic hepatitis B or C, irrespective of the presence of HCC. Serum levels of AST and ALT reflect hepatocellular damage, and higher hepatocellular damage generally induces a higher wound healing response. Thus, our current findings may be in line with our speculation that plasma ADAMTS13 activity or antigen level reflects the activity of hepatic stellate cells as a main effector of wound healing and fibrosis in the liver.

Major finding of this study is that the higher plasma ADAMTS13 activity or antigen level was a significant risk factor for HCC development. With regard to HCC development among patients with chronic hepatitis B or C without the past history of HCC, plasma ADAMTS13 activity was higher in the patients who developed HCC than in those who did not develop HCC. Among the various clinical parameters, univariate analysis revealed that the higher plasma ADAMTS13 activity was a significant risk factor for HCC development. Then, multivariate analysis showed that the higher plasma ADAMTS13 activity was a significantly predicting factor for hepatocarcinogenesis, independent of other significant risk factors for HCC development, including the variables predicting the stage of liver fibrosis. This potential link between plasma ADAMTS13 activity and HCC development was further observed in the analysis of HCC recurrence: the patients who had HCC recurrence during the 1-year follow-up period had also significantly higher plasma ADAMTS13 activity or antigen level than those who did not have HCC recurrence. Then, only plasma ADAMTS13 activity or antigen level was retained in the multivariate Cox proportional hazard model as a significant risk factor of recurrence.

Published OnlineFirst August 29, 2011; DOI:10.1158/1055-9965.EPI-11-0464

Then, we wondered how HCC development might be predictable by the activity or antigen level of plasma ADAMTS13, whose source is mainly hepatic stellate cells, as a key player of liver fibrosis. To explain this, the notion that advanced liver fibrosis is the strong risk factor for HCC development (17) may be important. Furthermore, the recent evidence suggests a potential direct link between hepatic stellate cells and HCC (3), as follows.

It is well known that HCC usually develops in the liver already suffering from chronic liver disease (2). In particular, HCV-related cirrhosis is associated with an extremely high risk of HCC development, with a reported annual incidence ranging between 3% and 8% (28–30). Thus, advanced liver fibrosis is one of the strongest risk factors for HCC development. In fact, the higher liver stiffness value is reportedly a strong risk for HCC development (21). In this study, a significant correlation was observed between plasma ADAMTS13 activity or antigen level and the variables predicting the stage of liver fibrosis such as liver stiffness value. Thus, we have first speculated that plasma ADAMTS13 activity is retained as a risk factor for HCC development by univariate analysis because plasma ADAMTS13 activity may reflect liver fibrosis. However, the higher plasma ADAMTS13 activity was a significant risk factor for HCC development, independent of liver stiffness value by multivariate analysis. Furthermore, in the analysis of HCC recurrence, plasma ADAMTS13 activity or antigen level was retained as a significant risk for HCC development, but not liver stiffness value, by multivariate analysis. The current finding that plasma ADAMTS13 activity or antigen level significantly correlated with serum AST and ALT levels may explain this. Of note, it was previously shown that the higher serum ALT is associated with the higher rate of incidence of HCC development (31) and HCC recurrence after the surgical treatment (32) in HCV-related cirrhosis, suggesting that more hepatocellular damage increases a risk for HCC development in the liver of the same stage of fibrosis. Because plasma ADAMTS13 activity or antigen level reflect hepatocellular damage and subsequent wound healing as well as liver fibrosis stage, plasma ADAMTS13 activity, or antigen level may act distinctly from liver stiffness value in the risk analysis of HCC development.

Alternatively, the prediction of HCC development by plasma ADAMTS13 activity or antigen level may be explained by a potential direct link between hepatic stellate cells and HCC, which has been recently reported (3). This concept is suggested based on the findings that hepatic stellate cells express the stem cell marker of CD133 (33) and both hedgehog (34, 35) and Wnt signaling (36) are found in hepatic stellate cells, two pathways implicated in stem cell differentiation and cancer (37). Furthermore, the direct promotion of tumorigenicity of HCC by hepatic stellate cells has been reported (38).

In human studies, the alteration of plasma ADAMTS13 activity in chronic liver disease has already been reported (39–44). In patients with liver cirrhosis, plasma ADAMTS13 activity was shown to be decreased (39) in relation to the severity of cirrhosis (44), although the wide range of values were detected compared with normal controls (43). In contrast, Lisman and colleagues showed that plasma ADAMTS13 activity in patients with liver cirrhosis was highly variable and not significantly different from that in normal controls (42). In line with the latter report, plasma ADAMTS13 activity in chronic hepatitis B and C was variable in the current study. We speculate that these distinct results of plasma ADAMTS13 activity in chronic liver disease may be caused by the characteristics of the patients enrolled in the analysis. The patients with reduced plasma ADAMTS13 activity in the previous reports (39, 43, 44) might have minimal hepatitis activity, that is, minimal wound healing response. Highly variable activity of plasma ADAMTS13 in liver cirrhosis (42) might also be explained by the variable hepatitis activity in those patients. This issue should be further clarified.

In conclusion, the higher plasma ADAMTS13 activity or antigen level was a significantly independent risk factor for HCC development in chronic hepatitis B or C, suggesting that plasma ADAMTS13 activity and antigen level may be useful in the prediction of hepatocarcinogenesis in chronic liver disease. It should be further evaluated whether plasma ADAMTS13 activity and antigen level could be useful as a predictor of HCC development with a larger sample size and also with other etiology of underlying chronic liver disease such as NASH.

Disclosure of Potential Conflicts of Interest

No potential conflicts of interest were disclosed.

Grant Support

This work was supported by Kurozumi Medical Foundation Fund.

The costs of publication of this article were defrayed in part by the payment of page charges. This article must therefore be hereby marked *advertisement* in accordance with 18 U.S.C. Section 1734 solely to indicate this fact.

Received May 18, 2011; revised August 19, 2011; accepted August 20, 2011; published OnlineFirst August 29, 2011.

References

1. Dvorak HF. Tumors: wounds that do not heal. Similarities between tumor stroma generation and wound healing. N Engl J Med 1986;315:1650–9.
2. Llovet JM, Burroughs A, Bruix J. Hepatocellular carcinoma. Lancet 2003;362:1907–17.
3. Friedman SL. Mechanisms of hepatic fibrogenesis. Gastroenterology 2008;134:1655–69.
4. Furlan M, Robles R, Solenthaler M, Wassmer M, Sandoz P, Lammle B. Deficient activity of von Willebrand factor-cleaving protease in chronic relapsing thrombotic thrombocytopenic purpura. Blood 1997;89:3097–103.
5. Kinoshita S, Yoshioka A, Park YD, Ishizashi H, Konno M, Funato M, et al. Upshaw-Schulman syndrome revisited: a concept of

Published OnlineFirst August 29, 2011; DOI:10.1158/1055-9965.EPI-11-0464

congenital thrombotic thrombocytopenic purpura. Int J Hematol 2001;74:101–8.
6. Sasahara Y, Kumaki S, Ohashi Y, Minegishi M, Kano H, Bessho F, et al. Deficient activity of von Willebrand factor-cleaving protease in patients with Upshaw-Schulman syndrome. Int J Hematol 2001;74:109–14.
7. Zheng X, Chung D, Takayama TK, Majerus EM, Sadler JE, Fujikawa K. Structure of von Willebrand factor-cleaving protease (ADAMTS13), a metalloprotease involved in thrombotic thrombocytopenic purpura. J Biol Chem 2001;276:41059–63.
8. Soejima K, Mimura N, Hirashima M, Maeda H, Hamamoto T, Nakagaki T, et al. A novel human metalloprotease synthesized in the liver and secreted into the blood: possibly, the von Willebrand factor-cleaving protease? J Biochem (Tokyo) 2001;130:475–80.
9. Cal S, Obaya AJ, Llamazares M, Garabaya C, Quesada V, Lopez-Otin C. Cloning, expression analysis, and structural characterization of seven novel human ADAMTSs, a family of metalloproteinases with disintegrin and thrombospondin-1 domains. Gene 2002;283:49–62.
10. Zhou W, Inada M, Lee TP, Benten D, Lyubsky S, Bouhassira EE, et al. ADAMTS13 is expressed in hepatic stellate cells. Lab Invest 2005;85: 780–8.
11. Uemura M, Tatsumi K, Matsumoto M, Fujimoto M, Matsuyama T, Ishikawa M, et al. Localization of ADAMTS13 to the stellate cells of human liver. Blood 2005;106:922–4.
12. Kume Y, Ikeda H, Inoue M, Tejima K, Tomiya T, Nishikawa T, et al. Hepatic stellate cell damage may lead to decreased plasma ADAMTS13 activity in rats. FEBS Lett 2007;581:1631–4.
13. Watanabe N, Ikeda H, Kume Y, Satoh Y, Kaneko M, Takai D, et al. Increased production of ADAMTS13 in hepatic stellate cells contributes to enhanced plasma ADAMTS13 activity in rat models of cholestasis and steatohepatitis. Thromb Haemost 2009;102:389–96.
14. Liu L, Choi H, Bernardo A, Bergeron AL, Nolasco L, Ruan C, et al. Platelet-derived VWF-cleaving metalloprotease ADAMTS-13. J Thromb Haemost 2005;3:2536–44.
15. Turner N, Nolasco L, Tao Z, Dong JF, Moake J. Human endothelial cells synthesize and release ADAMTS-13. J Thromb Haemost 2006;4: 1396–404.
16. Manea M, Kristoffersson A, Schneppenheim R, Saleem MA, Mathieson PW, Morgelin M, et al. Podocytes express ADAMTS13 in normal renal cortex and in patients with thrombotic thrombocytopenic purpura. Br J Haematol 2007;138:651–62.
17. El-Serag HB, Marrero JA, Rudolph L, Reddy KR. Diagnosis and treatment of hepatocellular carcinoma. Gastroenterology 2008;134: 1752–63.
18. Kato S, Matsumoto M, Matsuyama T, Isonishi A, Hiura H, Fujimura Y. Novel monoclonal antibody-based enzyme immunoassay for determining plasma levels of ADAMTS13 activity. Transfusion 2006;46: 1444–52.
19. Castera L, Vergniol J, Foucher J, Le Bail B, Chanteloup E, Haaser M, et al. Prospective comparison of transient elastography, Fibrotest, APRI, and liver biopsy for the assessment of fibrosis in chronic hepatitis C. Gastroenterology 2005;128:343–50.
20. Ziol M, Handra-Luca A, Kettaneh A, Christidis C, Mal F, Kazemi F, et al. Noninvasive assessment of liver fibrosis by measurement of stiffness in patients with chronic hepatitis C. Hepatology 2005;41:48–54.
21. Masuzaki R, Tateishi R, Yoshida H, Goto E, Sato T, Ohki T, et al. Prospective risk assessment for hepatocellular carcinoma development in patients with chronic hepatitis C by transient elastography. Hepatology 2009;49:1954–61.
22. Torzilli G, Minagawa M, Takayama T, Inoue K, Hui AM, Kubota K, et al. Accurate preoperative evaluation of liver mass lesions without fine-needle biopsy. Hepatology 1999;30:889–93.
23. Teratani T, Yoshida H, Shiina S, Obi S, Sato S, Koike Y, et al. A novel display of reconstruction computed tomography for the detection of small hepatocellular carcinoma. Liver Int 2004;24:619–24.
24. Fujishima T, Yoshida H, Obi S, Shiina S, Kanda M, Tateishi R, et al. Analysis of factors influencing hepatocellular carcinoma detection: efficient use of computed tomography during arterial portography and during hepatic arteriography. J Gastroenterol 2005;40:266–73.
25. Omata M, Tateishi R, Yoshida H, Shiina S. Treatment of hepatocellular carcinoma by percutaneous tumor ablation methods: Ethanol injection therapy and radiofrequency ablation. Gastroenterology 2004;127: S159–66.
26. Ikeda K, Saitoh S, Suzuki Y, Kobayashi M, Tsubota A, Fukuda M, et al. Interferon decreases hepatocellular carcinogenesis in patients with cirrhosis caused by the hepatitis B virus: a pilot study. Cancer 1998;82: 827–35.
27. Kasahara A, Hayashi N, Mochizuki K, Takayanagi M, Yoshioka K, Kakumu S, et al. Risk factors for hepatocellular carcinoma and its incidence after interferon treatment in patients with chronic hepatitis C. Osaka Liver Disease Study Group. Hepatology 1998;27:1394–402.
28. Yoshida H, Shiratori Y, Moriyama M, Arakawa Y, Ide T, Sata M, et al. Interferon therapy reduces the risk for hepatocellular carcinoma: national surveillance program of cirrhotic and noncirrhotic patients with chronic hepatitis C in Japan. IHIT Study Group. Inhibition of hepatocarcinogenesis by interferon therapy. Ann Intern Med 1999;131:174–81.
29. Tsukuma H, Hiyama T, Tanaka S, Nakao M, Yabuuchi T, Kitamura T, et al. Risk factors for hepatocellular carcinoma among patients with chronic liver disease. N Engl J Med 1993;328:1797–801.
30. Ikeda K, Saitoh S, Koida I, Arase Y, Tsubota A, Chayama K, et al. A multivariate analysis of risk factors for hepatocellular carcinogenesis: a prospective observation of 795 patients with viral and alcoholic cirrhosis. Hepatology 1993;18:47–53.
31. Tarao K, Rino Y, Ohkawa S, Shimizu A, Tamai S, Miyakawa K, et al. Association between high serum alanine aminotransferase levels and more rapid development and higher rate of incidence of hepatocellular carcinoma in patients with hepatitis C virus-associated cirrhosis. Cancer 1999;86:589–95.
32. Tarao K, Takemiya S, Tamai S, Sugimasa Y, Ohkawa S, Akaike M, et al. Relationship between the recurrence of hepatocellular carcinoma (HCC) and serum alanine aminotransferase levels in hepatectomized patients with hepatitis C virus-associated cirrhosis and HCC. Cancer 1997;79:688–94.
33. Kordes C, Sawitza I, Muller-Marbach A, Ale-Agha N, Keitel V, Klonowski-Stumpe H, et al. CD133+ hepatic stellate cells are progenitor cells. Biochem Biophys Res Commun 2007;352:410–7.
34. Sicklick JK, Li YX, Choi SS, Qi Y, Chen W, Bustamante M, et al. Role for hedgehog signaling in hepatic stellate cell activation and viability. Lab Invest 2005;85:1368–80.
35. Yang L, Wang Y, Mao H, Fleig S, Omenetti A, Brown KD, et al. Sonic hedgehog is an autocrine viability factor for myofibroblastic hepatic stellate cells. J Hepatol 2008;48:98–106.
36. Myung SJ, Yoon JH, Gwak GY, Kim W, Lee JH, Kim KM, et al. Wnt signaling enhances the activation and survival of human hepatic stellate cells. FEBS Lett 2007;581:2954–8.
37. Taipale J, Beachy PA. The Hedgehog and Wnt signalling pathways in cancer. Nature 2001;411:349–54.
38. Amann T, Bataille F, Spruss T, Muhlbauer M, Gabele E, Scholmerich J, et al. Activated hepatic stellate cells promote tumorigenicity of hepatocellular carcinoma. Cancer Sci 2009;100:646–53.
39. Mannucci PM, Canciani MT, Forza I, Lussana F, Lattuada A, Rossi E. Changes in health and disease of the metalloprotease that cleaves von Willebrand factor. Blood 2001;98:2730–5.
40. Kavakli K, Canciani MT, Mannucci PM. Plasma levels of the von Willebrand factor-cleaving protease in physiological and pathological conditions in children. Pediatr Hematol Oncol 2002;19:467–73.
41. Uemura M, Matsuyama T, Ishikawa M, Fujimoto M, Kojima H, Sakurai S, et al. Decreased activity of plasma ADAMTS13 may contribute to the development of liver disturbance and multiorgan failure in patients with alcoholic hepatitis. Alcohol Clin Exp Res 2005;29:264S–71S.
42. Lisman T, Bongers TN, Adelmeijer J, Janssen HL, de Maat MP, de Groot PG, et al. Elevated levels of von Willebrand factor in cirrhosis support platelet adhesion despite reduced functional capacity. Hepatology 2006;44:53–61.
43. Feys HB, Canciani MT, Peyvandi F, Deckmyn H, Vanhoorelbeke K, Mannucci PM. ADAMTS13 activity to antigen ratio in physiological and pathological conditions associated with an increased risk of thrombosis. Br J Haematol 2007;138:534–40.
44. Uemura M, Fujimura Y, Matsumoto M, Ishizashi H, Kato S, Matsuyama T, et al. Comprehensive analysis of ADAMTS13 in patients with liver cirrhosis. Thromb Haemost 2008;99:1019–29.

nature COMMUNICATIONS

ARTICLE

Received 30 Mar 2011 | Accepted 11 May 2011 | Published 7 Jun 2011

DOI:10.1038/ncomms1345

MicroRNA122 is a key regulator of α-fetoprotein expression and influences the aggressiveness of hepatocellular carcinoma

Kentaro Kojima[1,*], Akemi Takata[1,*], Charles Vadnais[2,*], Motoyuki Otsuka[1], Takeshi Yoshikawa[1], Masao Akanuma[3], Yuji Kondo[1], Young Jun Kang[4], Takahiro Kishikawa[1], Naoya Kato[5], Zhifang Xie[6], Weiping J. Zhang[6], Haruhiko Yoshida[1], Masao Omata[1], Alain Nepveu[2] & Kazuhiko Koike[1]

α-fetoprotein (AFP) is not only a widely used biomarker in hepatocellular carcinoma (HCC) surveillance, but is also clinically recognized as linked with aggressive tumour behaviour. Here we show that deregulation of microRNA122, a liver-specific microRNA, is a cause of both AFP elevation and a more biologically aggressive phenotype in HCC. We identify CUX1, a direct target of microRNA122, as a common central mediator of these two effects. Using liver tissues from transgenic mice in which microRNA122 is functionally silenced, an orthotopic xenograft tumour model, and human clinical samples, we further demonstrate that a microRNA122/CUX1/microRNA214/ZBTB20 pathway regulates AFP expression. We also show that the microRNA122/CUX1/RhoA pathway regulates the aggressive characteristics of tumours. We conclude that microRNA122 and associated signalling proteins may represent viable therapeutic targets, and that serum AFP levels in HCC patients may be a surrogate marker for deregulated intracellular microRNA122 signalling pathways in HCC tissues.

[1] Department of Gastroenterology, Graduate School of Medicine, The University of Tokyo, Tokyo 113-8655, Japan. [2] Goodman Cancer Center and Departments of Oncology, Biochemistry and Medicine, McGill University, Montreal, Quebec H3A 1A3, Canada. [3] Division of Gastroenterology, The Institute for Adult Diseases, Asahi Life Foundation, Tokyo 100-0005, Japan. [4] Department of Immunology and Microbial Science, The Scripps Research Institute, La Jolla, California 92037, USA. [5] Unit of Disease Control Genome Medicine, The Institute of Medical Science, The University of Tokyo, Tokyo 108-8639, Japan. [6] Department of Pathophysiology, Second Military Medical University, Shanghai 200433, China. *These authors contributed equally to this work. Correspondence and requests for materials should be addressed to M. Otsuka (email: otsukamo-tky@umin.ac.jp).

The incidence of hepatocellular carcinoma (HCC), the third most common cause of cancer-related mortality worldwide[1], is currently increasing[2]. The recent discovery of the efficacy of sorafenib, a multikinase inhibitor, as a treatment for patients with advanced HCC, has represented a major breakthrough in the clinical management, although the survival benefit has been shown to be less than 3 months[3]. No other effective therapy is currently available for patients with advanced disease[4]. As such, there is a continuing need to develop novel therapeutics and approaches for treatment of advanced HCC[5].

To develop targeted cancer therapies, we must first identify aberrantly regulated molecular pathways specific to this cancer. Clinically, it is also important to discover useful and convenient surrogate serum biomarkers that reflect aberrations in molecular pathways due to the molecular mechanisms of their expression, to identify the deregulated intracellular signalling pathways and to spare the patients from invasive clinical tests.

Currently, α-fetoprotein (AFP) is the most widely used serum biomarker for HCC surveillance[6]. Although the regulation of AFP gene expression is not fully understood, p53 (ref. 7), β-catenin[8] and the recently identified zinc-finger protein, ZBTB20 (ref. 9), have been reported to be involved. Furthermore, whereas mounting clinical evidence indicates that AFP elevation is linked to a more aggressive tumour phenotype characterized by vascular invasion, metastasis and poor differentiation[10,11], it remains to be determined whether the two phenotypes represent anything more than coincidental epiphenomena[12].

MicroRNAs (miRNAs) are short, single-stranded, non-coding RNAs. Although first identified in *Caenorhabditis elegans*[13], miRNAs are now known to be expressed in most organisms, from plants to vertebrates[14]. Primary miRNAs, which possess stem-loop structures, are processed into mature miRNAs by Drosha and Dicer RNA polymerase III. These mature miRNAs then associate with the RNA-induced silencing complex, and the resulting complex directly binds to the 3′-untranslated regions of target messenger RNAs to act as suppressors of translation and gene expression. Thus, depending on the target mRNAs, miRNAs are responsible for the control of various biological functions including cell proliferation, apoptosis, differentiation, metabolism, oncogenesis and oncogenic suppression[15–17].

MiRNA122 (miR122) is a tissue-specific miRNA that is most abundant in the liver[18], wherein it is responsible for the maintenance of fatty acid metabolism[19,20] and circadian rhythms[21]. As shown for other tissue-specific miRNAs[22], expression of miR122 has been reported to be downregulated in carcinomas, particularly in more malignant tumours, although these results remain controversial because of conflicting reports[23–26]. The biological significance of the downregulation of miR122 expression in HCC at the molecular level has not yet been fully elucidated.

In the present study, we explored the role of microR122 in HCC by silencing it both in human HCC cells and in a transgenic mouse model. Our molecular analysis enabled us to define the complex regulatory cascades underlying the clinically recognized link between raised AFP levels and a more aggressive phenotype in HCC.

Results

Establishment of miR122-silenced HCC cell lines. To characterize the functional consequences of miR122 downregulation in HCC cells, Huh7 and PLC/PRF/5 cells were stably transduced with a lentivirus that expresses RNA hairpins that produce mature antisense RNA designed to silence miR122 function. These cells were selected on the basis of their relatively high levels of miR122 expression[24,27]. Several mismatches were intentionally inserted into the RNA hairpin sequences to produce more stable templates for miR122 binding and sequestration and to perturb the participation of miR122 in RNA-induced silencing complex-associated inhibition of translation (Fig. 1a).

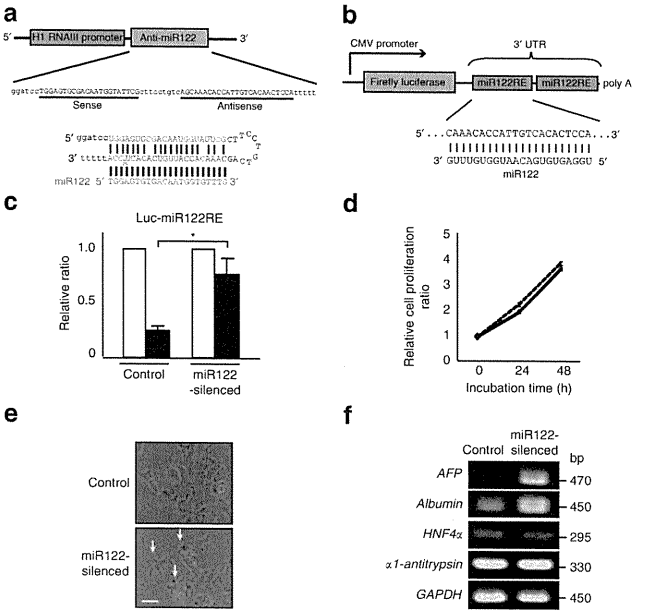

Figure 1 | Establishment of miR122-silenced HCC cell lines. (**a**), The miRZip122 construct, which yields a functional single-stranded full-length antisense miRNA complementary o miR122, processed from a stem-loop-stem molecule and transcribed from the constitutively active H1 RNA III promoter. Several mismatched nucleotides were included to efficiently produce a single-stranded antisense miR122 molecule. (**b**) Schematic representation of the luciferase reporter used to examine miR122 activity. The firefly luciferase gene, driven by a cytomegalovirus (CMV) promoter, contains two tandem miR122-binding sites (miR122-responsive elements; miR122-RE) in its 3′-UTR. (**c**) The suppressive effects of miR122 precursor expression (black bar) on luciferase activity in control and miR122-silenced cells. Test values were normalized to those obtained from the cells transfected with a miRNA precursor-non-expressing empty vector (white bar), which were set to 1. Data represent the mean±s.d. of three independent experiments using Huh7 cells. $^*P<0.05$ (*t*-test). Similar results were obtained using PLC/PRF/5 cells. (**d**) Control (solid line) and miR122-silenced cells (dashed line) were plated at a density of 2×10^4 cells per well. After incubation for 24 and 48 h, numbers of cells were calculated as described in the Methods. Data represent the mean±s.d. of three independent experiments using Huh7 cells. Similar results were obtained using PLC/PRF/5 cells. (**e**) Changes in cellular morphology of Huh7 miR122-silenced cells are shown. Arrows indicate pseudopodia. Scale bar, 50 μm. Similar phenotypes were observed using PLC/PRF/5 cells. (**f**) The expression of several hepatocyte markers in control and Huh7 miR122-silenced cells was evaluated by semi-quantitative RT-PCR. Representative results from three independent experiments using Huh7 cells are shown. Similar results were obtained using PLC/PRF/5 cells.

To confirm effective miR122 silencing in transduced cells, we analysed the luciferase activity of reporters containing miR122-binding sites (the function of which is suppressed by miR122 overexpression) (Fig. 1b) in miR122-silenced and control cells. As expected, overexpression of the miR122 precursor greatly suppressed luciferase activity in control cells (Fig. 1c). In contrast, this suppressive effect was significantly reduced in miR122-silenced cells (Fig. 1c), indicating that miR122 was indeed functionally silenced.

To characterize the biological changes that result from the loss of miR122 function, we next analysed cell proliferation, morphology and differentiation in miR122-silenced cells. The rates of cell

proliferation were comparable between control and silenced cells (Fig. 1d); however, miR122-silenced cells exhibited a larger number of distinct pseudopodia (Fig. 1e). Next, as miR122 is specifically expressed in the liver, we hypothesized that it may have a role in hepatocyte differentiation and, therefore, we investigated the expression of several hepatocyte markers by semi-quantitative RT–PCR. We observed an increase in AFP expression and a slight elevation of albumin expression in miR122-silenced cells, but the expression levels of other hepatocyte markers, such as hepatocyte nuclear factor 4α (HNF4α) and α_1-antitrypsin, did not change (Fig. 1f).

MiR122-silenced HCC cells exhibit a more invasive phenotype. Because miR122-silenced cells exhibited an increased number of pseudopodia, we next characterized phenotypes associated with more biologically aggressive cell characteristics. We found that actin polymerization and pseudopod formation were significantly increased in miR122-silenced cells (Fig. 2a). The increase in the number of pseudopodia was confirmed by a quantitative pseudopodia assay (Supplementary Fig. S1). Although the expression levels of the mesenchymal marker α-smooth muscle actin were only slightly increased, we observed a significant decrease in the expression of the epithelial marker E-cadherin in miR122-silenced cells (Fig. 2b). Furthermore, the expression of other epithelial-to-mesenchymal transition markers such as fibronectin, N-cadherin, snail and Zeb1 was altered in miR122-silenced cells (Supplementary Fig. S1). These findings are consistent with the notion that loss of miR122 function leads to a more malignant phenotype.

We next performed scratch and invasion assays to characterize the invasive phenotype of miR122-silenced cells. Rates of cell migration and of cell invasion were significantly increased in miR122-silenced cells (Fig. 2c,d). As the proliferation rates of control and miR122-silenced cells were similar (Fig. 1d), altogether these results suggest that inhibition of miR122 function in HCC cells may lead to increases in malignancy-related cellular properties.

To investigate the molecular mechanisms underlying these cellular phenotypes, we assessed the activity of RhoA and Rac1, which are small GTPases that are closely associated with cell migration and invasion[28]. Although Rac1 activity did not significantly change, RhoA activity significantly increased in miR122-silenced cells (Fig. 2e), suggesting that the increase in cell migration and invasion in miR122-silenced cells may result from increased RhoA activity.

AFP expression is increased in miR122-silenced HCC cells. As we observed an increase in AFP expression in miR122-silenced cells (Fig. 1f), we next sought to quantify AFP concentrations in culture supernatants using an enzyme-linked immunosorbent assay (ELISA). AFP levels were approximately three times higher in the supernatant of miR122-silenced cells as compared with control cells (Fig. 3a). Consistent with this observation, immunofluorescence staining for AFP produced a stronger cytoplasmic signal and quantitative RT–PCR revealed a tenfold increase in AFP mRNA levels in miR122-silenced cells (Fig. 3b,c).

The 3′-UTR of the AFP mRNA did not contain predicted miR122 target sequences, based on sequence analyses performed using miRNA target search engines such as TargetScan (http://www.targetscan.org), suggesting that it is unlikely that miR122 directly regulates AFP expression. Therefore, to characterize the mechanisms underlying increased AFP expression in miR122-silenced cells, we first assessed the stability of the AFP mRNA in miR122-silenced cells. As expected, AFP mRNA stability was unaffected by silencing of miR122, as the amount of mRNA was comparable between control and miR122-silenced cells at 6, 12 and 24 h after inhibition of new transcription by treatment with actinomycin D (Fig. 3d). The increase in AFP mRNA levels in the absence of changes in mRNA stability suggested that transcription of AFP was increased

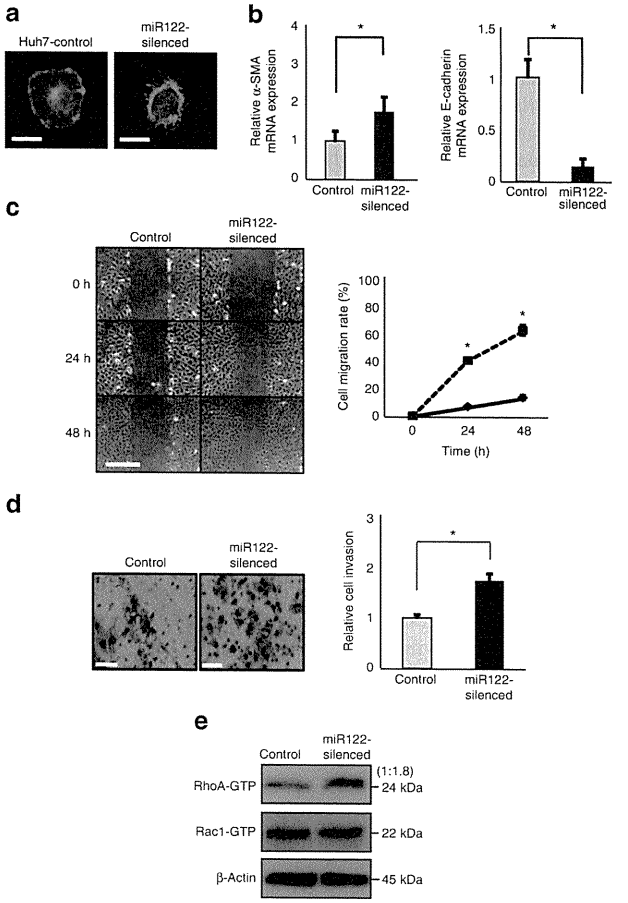

Figure 2 | HCC cells silenced for miR122 function exhibit a more invasive phenotype. (**a**) Cells were treated with 2 ng ml^{-1} TGF-β for 12 h, and actin filaments were stained with Alexa Fluor 488-conjugated phalloidin. Representative results from two independent experiments using Huh7 cells are shown. Similar results were obtained using PLC/PRF/5 cells. Scale bar, 50 μm. (**b**) Expression levels of α–smooth muscle actin and E-cadherin mRNAs were assessed by quantitative RT–PCR. Values shown represent mRNA expression levels in experimental cells relative to control cells. Data represent the mean±s.d. of three independent experiments using Huh7 cells. *$P<0.05$ (*t*-test). Similar results were obtained for PLC/PRF/5 cells. (**c**) The degree of cell migration was characterized using a scratch assay. The ratio of migrating cells was significantly increased in miR122-silenced cells at 24 and 48 h after scratching. Left panels show representative images. Right panel shows the results from cell counts for four randomly chosen fields per experiment. Data are represented as the mean±s.d. of three experiments using Huh7 control (solid line) and miR122-silenced cells (dashed line). *$P<0.001$ (*t*-test). Similar results were obtained for PLC/PRF/5 cells. (**d**) The degree of cell invasion was examined using cell invasion chambers. Representative images of stained invaded cells (left). The relative cell invasion ratio after normalization to control cell invasion levels (right). Data represent the mean±s.d. of three independent experiments using Huh7 cells. Scale bar, 100 μm. *$P<0.01$ (*t*-test). Similar results were obtained for PLC/PRF/5 cells. (**e**) Rho and Rac1 activity was determined by comparing the amounts of active GTP-bound RhoA (RhoA-GTP) and Rac1 (Rac1-GTP) between control and miR122-silenced cells. The indicated numbers represent the relative expression levels. Equal loading in pull-down assays was confirmed by analysis of β-actin levels in the cell lysates. Representative results of five independent experiments using Huh7 cells are shown. Similar results were obtained using PLC/PRF/5 cells.